UCLouvain

epl

École polytechnique de Louvain

Fabrication of new aluminium frame for in-situ tensile testing in TEM

Author: **Christian OGANBULE**
Supervisors: **Hosni IDRISSI, Jean-Pierre RASKIN**
Readers: **Thomas PARDOEN, Michaël COULOMBIER**
Academic year 2020–2021
Master [120] in Chemical and Materials Engineering

Abstract

The in-depth characterization of thin films is important for the improvement of the performance of next generation Micro-Electro-Mechanical systems (MEMS) device. A straight-forward approach is to measure the tensile properties thin film. This approach combined with in-situ observation in TEM will deepen the understanding of the behavior of materials at nanoscale. Although, a wide range of solutions have been proposed for determining the mechanical properties of nano-structures and thin film, there is limited report on the tensile properties of thin films below 50nm. An aluminium frame have been fabricated in this work by optical lithography technique to ensure the transfer of an ultrathin tensile structure ($\sim 30nm$) onto a "Push-to-Pull" devices used for nanoscale tensile testing. This method have been applied for the in-situ tensile testing of copper thin film where a total strain of 0.107 [-] was observed.

Acknowledgements

In many ways, the next lines are dear to my heart because writing this thesis may seem to be an individual effort but in reality it is impossible without the much help received from those who have made this work possible. My first appreciation goes to my supervisors **Prof. Hosni Idrissi** and **Prof. Jean-Pierre Raskin.** Thank you for your presence and support throughout the entire process of working on this thesis.

I am grateful to **Dr. Michaël Coulombier** for his unending willingness to share from his wealth of knowledge of the micro and nano fabrication processes. Your decisive guidance at the most critical times during the thesis work does not go unnoticed. My sincere appreciation to my "buddy", **Alex Pip**. Thank you for always lifting my spirit during the long hours spent together at the WinFab.

I am indeed grateful to the members and staff at the WinFab facility of UCLouvain; **Sébastien Faniel, Christian Renaux, Nicola André, Romain Tuyaerts, Farzaneh Bahrami, Mohammad Wasil Malik and Sahar Jaddi**. Thank you for your various inputs at different fabrication process steps. Special thanks to **Dr. Marie-Stéphane Colla** for allowing me to use some space on your mask design and to **Prof. Thomas Pardeon** for taking time out of your busy schedule to read this thesis.

Special thanks to **Stijn Vandenbroeck, Ihtasham Ul Haq and Ankush Kashiwar** for assisting me with the last steps during this work. Lastly, I must appreciate my immediate family and close friends, especially **Tolulope Alo** for providing emotional support during what was indeed a "special" semester for me.

Contents

List of Figures

Chapter 1

Introduction

1.1 Motivation and objective of the work

The traditional approach to accessing the mechanical properties of engineering material involves the uniaxial pulling of the usually "large" test specimen, thereby measuring the corresponding displacement to an applied load. This is usually achieved in large machines that are commercially available and standardized by the ASTM international standards. The load is normalized by the gauge section while the displacement is converted to strain based on its ratio with the gauge length. The resulting stress-strain curve from such endeavor gives a description of mechanical properties such as elasticity, plasticity and fracture.

The understanding of the properties of materials at nano and micro scale has however been the interest of scientist and engineers over the years. It is interesting to realize that materials behave differently when scaled down to thin structures. As such, it is a worthy endeavor to investigate this size dependent properties in order to have a full grasp of the underlying physics. This understanding can then be employed to improve the numerous thin film application. Thin films find extensive application in the micro-electronics and semi-conductor industry as well as in the specific functionalization of surfaces. In general terms, thin films are fabricated either by chemical vapor deposition (CVD) or physical vapor deposition (PVD) methods either of which also influences the eventual property of the thin film. In fact, when in comes to mechanical properties of materials at micro or nano scale, there has not been a universal testing method. As such numerous testing methods have been proposed.

An interesting technology nowadays are the Micro-Electro-Mechanical systems otherwise known as MEMS technology. In general terms, they are defined as miniaturized mechanical and electro-mechanical devices or structures made by mocrofabrication techniques. The critical dimension of MEMS devices ranges from sub-micron at the lower band up to several millimeters at the upper band with a criterion of having some elements with mechanical functionality. The functional elements of MEMS devices includes miniaturized structures, sensors, actuators and microelectronics with the microsensors and microactuators being the most important. The microsensor and microactuators otherwise called transducers typically converts energy from one form to the other. For example, the microsensor converts mechanical signals into electrical signals. An extremely large number of micro machined sensors have been developed by researchers for typically every form of sensing possible which includes but not limited to temperature, pressure, inertial forces, chemical species magnetic fields and radiations. In fact, a number of the micromachined sensors have been found to outperform their macroscale counterparts and in addition to this exceptional performance, the batch fabrication technique used for their production translates to a low per-device production cost. As a consequence, it is possible to leverage on both the stellar device performance of MEMS devices as well as low cost level.

In order to therefore improve the performance of next generation of MEMS devices, there is need for in-depth characterization of thin films. One of the methods for obtaining such valuable information is by employing the use of in-situ tensile investigation in transmission electron microscope (TEM). This on its own can be challenging but advances in research on MEMS fabrication have led to several testing devices. Two common challenges for these methods of characterization are the preparation of suitable test samples and the manipulation and transfer of the prepared samples. The focus of this work is therefore the fabrication of a metallic frame that seeks to address the challenges associated with the transfer of prepared thin film samples unto a testing platform for *in-situ* tensile tensile testing in the TEM. This effort is part of a broader scientific interest in the in-depth understanding of the behaviour of thin film materials. In fact an attempt has been made previously by **Gillet** to fabricate a silicon frame for manipulation of tensile thin film [1]. This present work thus draws inspiration from his work with a bid to provide an optimization of the fabrication process.

1.2 General outline of the report

This report starts with a state of the art of the techniques used for mainly the uni-axial testing of thin films and nano-structures in **chapter two**. The review is divided into techniques that are based on the configuration of the testing devices. Some devices do not have a direct load sensor, others have a load sensor but require external actuation mechanisms while another class consists of a complete testing system having a direct load sensor and an on-chip actuator. A more simpler device configuration know as the lab-on-chip will also be briefly reviewed. The state-of-art is concluded by considering different methods for sample manipulation as wells as straining inside the TEM.

Chapter three details the process employed in this present work for the fabrication of an aluminum frame for better manipulation of ultra thin tensile samples for *in-situ* mechanical testing in the TEM. This chapter opens with a description of the design consideration for the aluminum frame before the detailing the fabrication process and ends with the demonstration of the transfer of tensile test thin film unto a testing platform.

Chapter four presents the main results of this thesis work with some further perspective that can be looked into. The results proves to be quite promising for the manipulation of ultra thin film structures onto a nano-testing platform.

Chapter 2

State of Art

2.1 Mechanical Testing of Nano-Scale Materials

Over the past decades, there have been an emergence of nanostructures with outstanding properties. Examples of these nanostructures include nanoparticles, nanowires, nanotubes and graphene. These devices have many important technological applications such as energy harvesting and storage [2, 3, 4], nanoelectromechanical systems (NEMS) [5, 6], flexible electronics [7, 8] and stretchable electronics [9, 10, 11]. Thus, measuring the mechanical properties of nanostructures is crucial for their intended application. In order to achieve this, a plethora of experimental testing methods have been developed with those based on MEMS showing great promise.

The most straight forward approach to accessing the mechanical properties of materials is to perform a tensile test which will be the major focus of this work. However, the challenges with mechanical characterization at nanoscale includes appropriate manipulation and positioning of specimen, measurement and application of nano-Newton forces as well as the measurement of local deformation with nanometer resolution [12]. Another challenge would be the direct real-time observation of deformed samples in order to deepen the knowledge of the deformation mechanisms at micro- and nano scale through quantitative measurements.

Figure 2.1 shows the common device configuration for nano-scale uniaxial testing. It can be observed that the same concepts used in testing machines for bulk samples have also been employed in this schematic. Typically, these testing machines consist of a

servohydraulic (MTS) or screw-driven (instron) actuator, a load cell (sensor) and a pair of grips. The methods of actuation, sensing and sample gripping are much different at the nano-scale. The testing device at nano-scale can therefore be grouped as those without a direct load sensor (figure 2.1a and b), having a direct load sensor and an external actuator (figure 2.1 c and d) and a complete testing system having a direct load sensor and an on-chip actuator (figure 2.1 e and f).

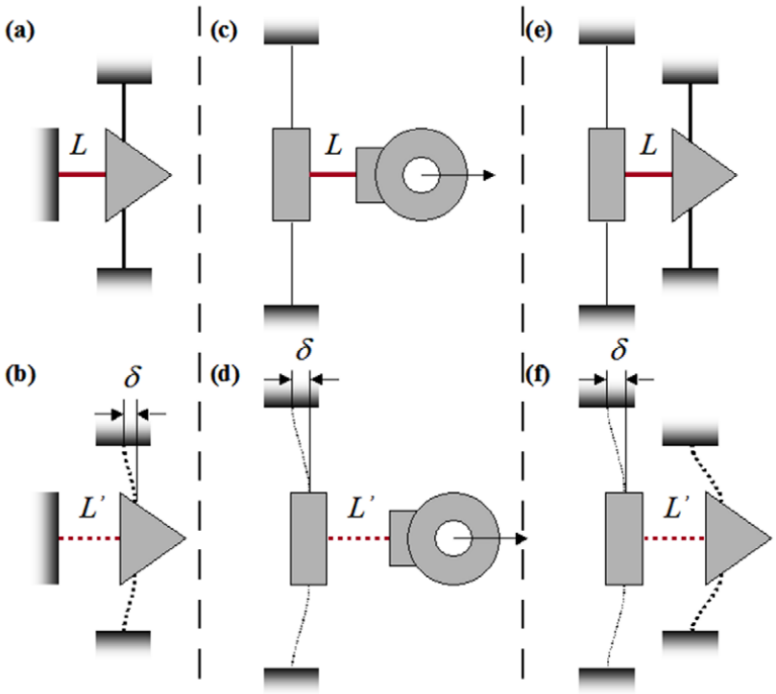

Figure 2.1: Common device configuration for nano-scale tensile testing [12]

In the first device configuration (figure 2.1a and b), the specimen is placed between the actuator (arrow shape) and the fixed post. The initial displacement (δ_0) of the actuator is measured based on the applied voltage and as the test proceeds $\delta(= L'$- L). The stress and strain can thus be extracted from the specimen load and displacement. The specimen displacement is same as δ while the load is defined as F = k_a $\times(\delta_0$ - $\delta)$. Where k_a is the spring constant of the actuator.

The test specimen is placed between the load sensor and gripping pad to which the external actuator is attached in the second device configuration (figure 2.1 c and d). The load applied on the specimen equates to the load on the sensor given as F = K_S $\times\delta$ where K_S and δ are the load sensor stiffness and displacement respectively. The same calculation is applied to the third device configuration (figure 2.1 e and f) with

the difference that there is an involvement of an on-chip actuator.

Different MEMS platform base on the three device configurations mentioned above will reviewed in the section 3.1, 2.1.2 and 2.1.3.

2.1.1 First device configuration

Based on the first device configuration, **Lu *et al*** fabricated a testing stage for the mechanics measurement of nano structures using a displacement controlled thermal actuator [13]. The stand alone device was fabricated using deep reactive ion etching (DRIE) as summarized in figure 2.2. A silicon device layer wafer was placed on a Boronfloat glass substrate by anodic bonding on which photoresist is patterned by photolithography. The silicon layer is then ected by DRIE followed by photoresist removal and then chromium and gold deposition. The electrical contacts where made after patterning of the chromium and gold layer by photolithography followed by the photoresist removal and a timed HF etching of the glass substrate. Then a connection between the device and the chip carrier was made.

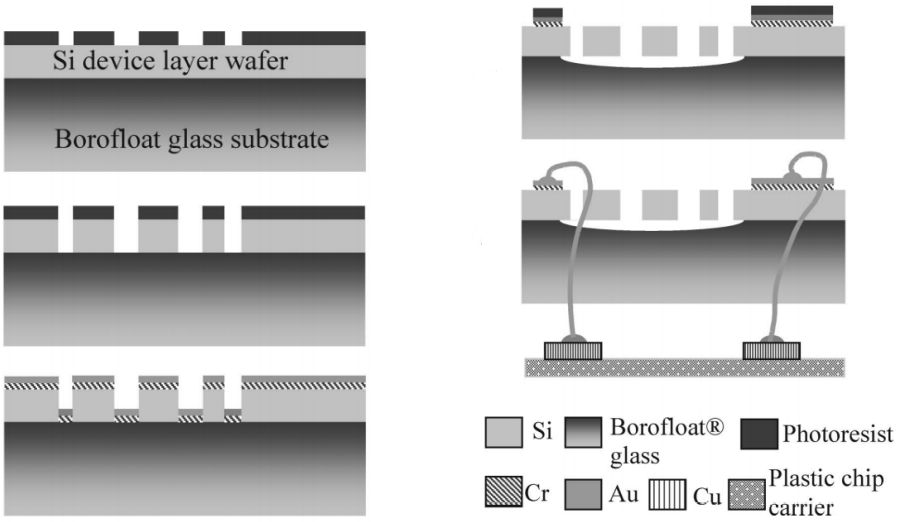

Figure 2.2: Step by step process for the device fabrication [13]

The idea of the design and fabrication of the device was to provide a controlled gap size between a movable and fixed part while measuring displacement and force with the aid of SEM imaging as shown in figure 2.3. In this case, the test specimen is transferred to the gap and clamped using electron-beam-induced decomposition or taking advantage of Van der Waals interactions. In principle, the thermal expanding beams expands

outward by Joule heating when electrical current is passed through them. This then translates to the motion of the V-shaped thin film on which the actuator is attached to its ends. The finished device had a working range from tens of nanometers up to 10 micrometers with displacements as small as 30nm per 10mA of input dc current. For an actuator displacement of 30nm and based on the mechanical models of the device a force of 0.27 µN was predicted.

In a separate work by **Lu *et al*** [14] the same platform was used perform *in situ* tensile testing on templated carbon nanotube (T-CNT) in a scanning electron microscope. The T-CNT was mounted by dielectrophoretic deposition and clamped by depositing a carbonaceous material by electron beam induced deposition (EBID). Deformation of the direct force-sensing beam gives an indication of the load on the specimen while pixel counting from the SEM images was used to compute the strain. A Young modulus of 14.6 ± 4.6 GPa was obtained for the T-CNT. Admittedly, the use of dielectophoresis is more scaleable when compared to the "pick-and-place" method for sample placement, it however suffers from a drawback of sample contamination. This will be discussed further in section 2.2.

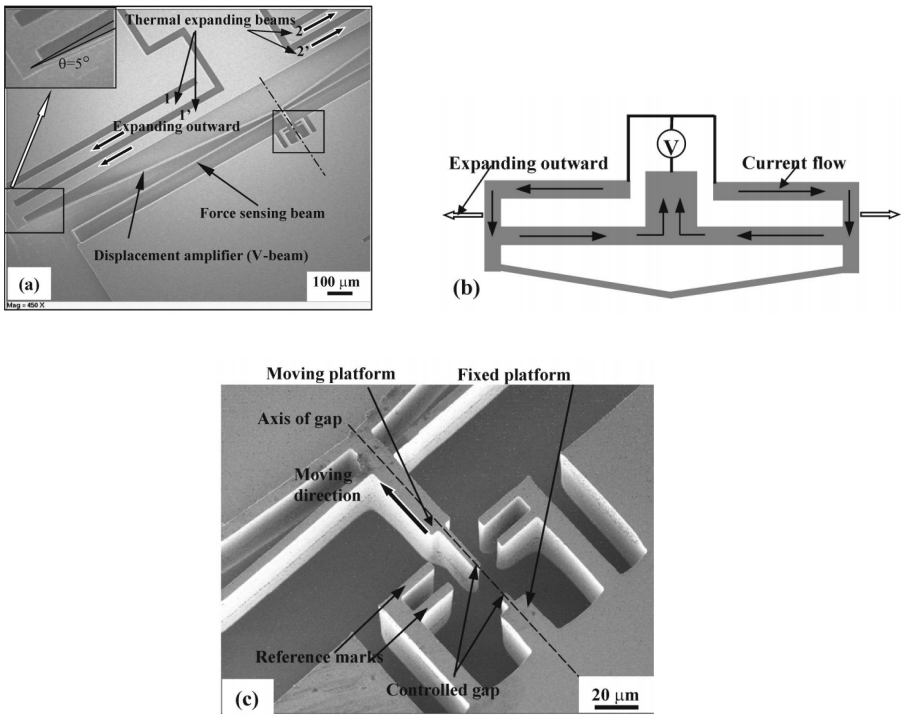

Figure 2.3: Schematic and SEM images of the fabricated device [13]

Kuichi *et al* measured the mechanical properties of carbon nanowires that were deposited by focused ion beam-assited chemical vapor deposition using an Electrostatic Actuated Nano Tensile testing device (EANATs) [15]. The actuators where made of 1000 - 5000 pairs of comb drive for stretching the nanowires by applying a biased voltage to the actuator (figure 2.4). A cantilever was built into the EANATs and the tensile load and displacement of the nanowires were measured based on the deflection of the cantilever in conjunction with a CCD camera firmly fixed on a stereomicroscope. The minimum resolution of 123 nN and 0.29 nm was observed as the tensile load and displacement respectively for the device. For the nanowires tested, an experimental average of 59.9 and 80.7 GPa was obtained as the Young's modulus and fracture stress respectively.

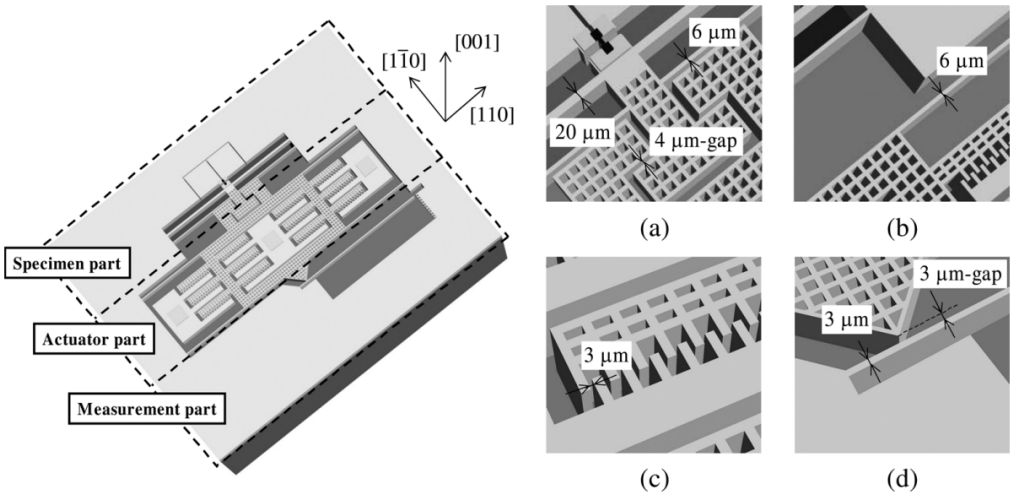

Figure 2.4: Schematic diagram of the EANAT (a) sample part (b) actuator part (c) electrostatic comb drive actuators (d) fixed end of the cantilever [15]

Brown *et al* designed and fabricated a microsystem for the electromechanial measurement of nanofibers [16]. The originality of the device was the simultaneous electrical and mechanical measurements performed on a conducting or semiconducting nanofiber. The design of the MEMS tensile testing system was such that it consists of fixed stage and a movable stage (figure 2.5) and fabricated using the PolyMUMPS process [17]. The moving stage is connected to a thermal actuator by a shuttle while the fixed stage is clamped to a silicon nitride substrate. An estimated output force of up to 400 µN was realized from the actuator based on its geometry and plane strain condition in solid mechanics. The test device was used to perform tensile measurements of a single crys-

tal gallium nitride nanowire [18]. Platinum-Carbon deposits formed in the SEM-FIB machine was used to clamp the nanowire to the MEMS structure by ion beam induced depostion (IBID). The drawback to this approach is the deposition of platinum on the specimen which may source of artifacts. The tested nanowires were found to exhibit a tensile strength ranging from 4.0 ± 1.7 GPa to 7.5 ± 3.4 GPa.

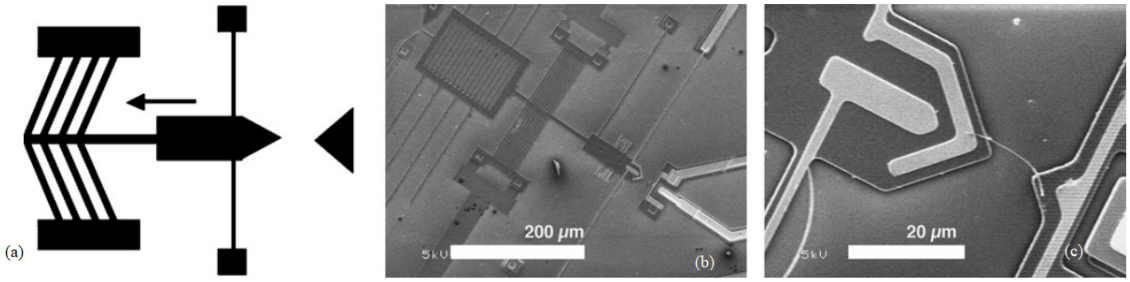

Figure 2.5: (a) Schematic image of the actuator and stage system. (b) SEM image of the overall device. (c) Zoomed in view of the device showing the mounted carbon nanotube. [16]

The "push-to-pull" concept has also gained popularity in the tensile testing of nano structures and has found practical application in MEMS platforms. Typically, the platform consists of an existing transducer (e.g. nanoindenter) and a micro-fabricated device that induces tension in the specimen when the device is compressed by the transducer. The push-to-pull platform that can be used in conjunction with a nanoindenter for *in situ* tensile testing in TEM was developed by Hystron Incorporated [19]. As shown in figure 2.6, the device has two parts, a fixed and a movable freestanding part which is supported by four folded beams. The nanoindenter is used to push the platform from the left side which increases the gap between the fixed and the and the movable part and thus translates to a tensile stress on the sample that is placed between the two parts. In the work of **Guo *et al***, the push-to-pull was used to observe the *in situ* elastic and structural phase transitions of 270nm wide VO_2 nanowires in TEM [20]. **Idrissi *et al*** also used the same device to perform nanomechanical testing on freestanding olivine beams (200nm thick) that was cut using the focused ion beam (FIB) [21]. The advantages and drawback of preparing the sample using FIB milling will be disscussed further in section 2.2.

Another type of push-to-pull platform was developed by Lu *et al* as shown in figure 2.6 [22]. The load indenter in this case converts compression to tensile stress in a direction perpendicular to the applied load direction. This device is also designed to be suitable

for *in situ* deformation in SEM and TEM and has been was used for *in situ* tensile testing on 360nm diameter nickel nanowire [23].

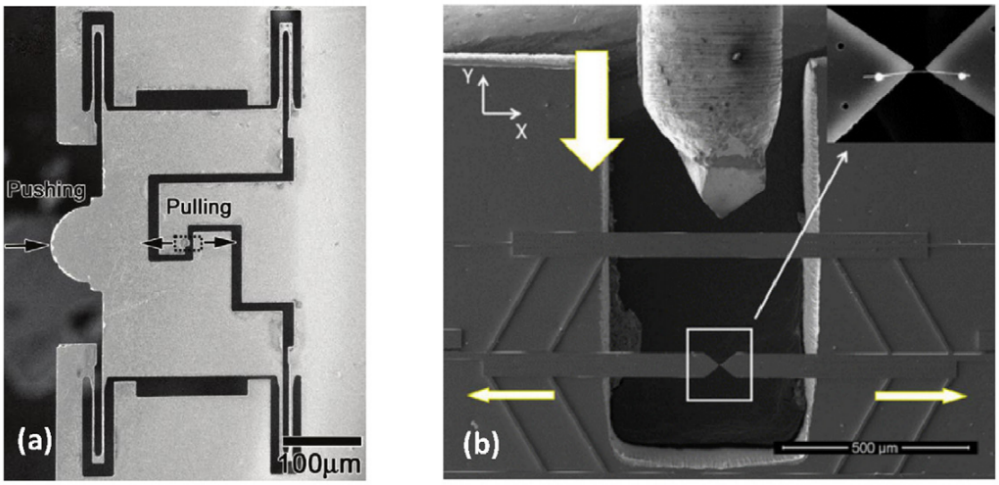

Figure 2.6: (a) SEM image of the push-to-pull device fabricated by Hystron [20] (b) SEM image of push-to-pull device by Lu *et al* [22].

Indeed the use of nano-scale testing platforms without a direct load sensor has the advantage of incorporating them with SEM and TEM for in-situ mechanical testing. As such in-depth information about the deformation mechanisms of materials can be accessed. The difficulty with the method remains the associated difficulties with sample manipulation, clamping and alignment as well as accurate measurement of load and displacement. It gets more complicated when the aim is to manipulate free standing test specimen lower than about 50nm because of the associated internal stresses and defects.

2.1.2 Second device configuration

A MEMS test device having an on-chip load sensor and external piezoelectric transducer was developed by **Naraghi *et al*** [24]. As shown if figure 2.7, the platform has a leaf-spring load sensor, a gripping pad and and a gap where the sample is mounted. The fixed end of the platform was achieved by using a tipless AFM cantilever attached to a three-axis stage. The measurement of the load and the displacement of polyacrylonitrile nanofibers (PAN) tested was recorded obtained from optical microscope using digital image correlation. This was because when polymeric fibers are subjected to SEM electron beams, they undergo physical ageing and cross-linking [25]. For the 300 to

600 nm diameter PAN specimen that was tested, an elastic modulus of 7.6 ± 1.5 GPa elastic modulus was measured with a huge irreversible strain exceeding 220%.

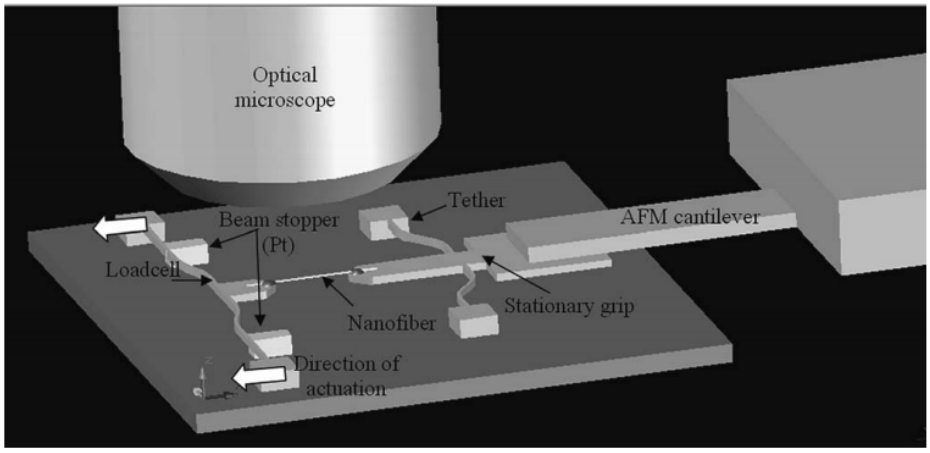

Figure 2.7: MEMS platform having a direct load sensor and an external piezoelectric transducer. [24]

The pioneering work of **Haque and Saif** brought about the use of MEMS platform to carry out *in situ* characterization of nanoscale thin films in SEM and TEM with varying environmental conditions of temperature and humidity [26]. The platform was fabricated by lithography and bulk machining of a silicon substrate. The set-up is composed of a load sensor, an external actuation mechanism and a co-fabricated free-standing specimen (figure 2.8). This is done to ensure perfect alignment and gripping thanks to the adhesive force between the silicon substrate and the test material. A U-shaped spring is also co-fabricated on the device to keep the structural integrity between the fixed and moving ends of the chip. Straining is achieved thanks to the holes on either side of the chip that fits to the mounting pins of the TEM stage. The stage was used to perform tensile testing on 200nm thick sputtered aluminum specimen measuring a yield stress up to 330 MPa and a Young modulus of 74.6 GPa.

2.1.3 Third device configuration

Zhu *et al* reported the MEMS platform that consist of both actuator and a load sensor for *in situ* tensile testing of nanostructures [27]. The interesting feature of the platform is the use of differential capacitance measurement for the load sensing. In essence, the displacement of the sensor is recorded by the measured capacitance change. As a consequence and from the knowledge of the stiffness of the sensor, the relationship between the load and the capacitance change can be obtained. Furthermore, the authors

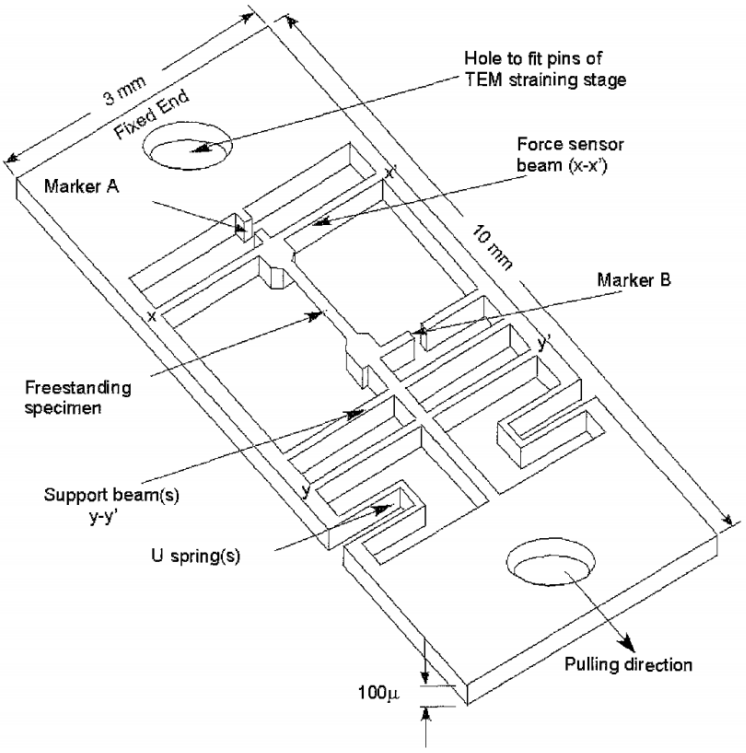

Figure 2.8: Schematic representation of the *in situ* tensile testing platform by Hauqe and Saif. [26]

designed the system with two types of actuators; thermal actuator and comb drive actuator (figure 2.9). The thermal actuator works in displacement control mode while the comb drive actuator works in force control mode. The device was used to perform *in situ* tensile testing on freestanding polySi films, palladium nanowires and carbon nanotubes [28].

The same kind of system developed by **Zhu *et al*** was used by **Cheng *et al*** to investigate the mechanical properties of silicon carbide (SiC) [29] and silver nanowires [30]. In their work on silver nanowires, the dislocation-mediated, time-dependent and fully reversible plastic behaviour of penta-twinned silver nanowires was investigate by *in-situ* tensile experiments in scanning and transmission electron microscope. Stress relaxation and complete plastic recovery was observed in the penta-twinned silver nanowires during loading and unloading respectively. A similar testing platform was developed by **Steighner *et al*** having a V-shaped thermal actuator and a capacitive load sensor. The platform was used to perform uniaxial tension loading of silicon nanowires in order to investigate size-dependent strength of silicon nanowires ranging between 268 to 840

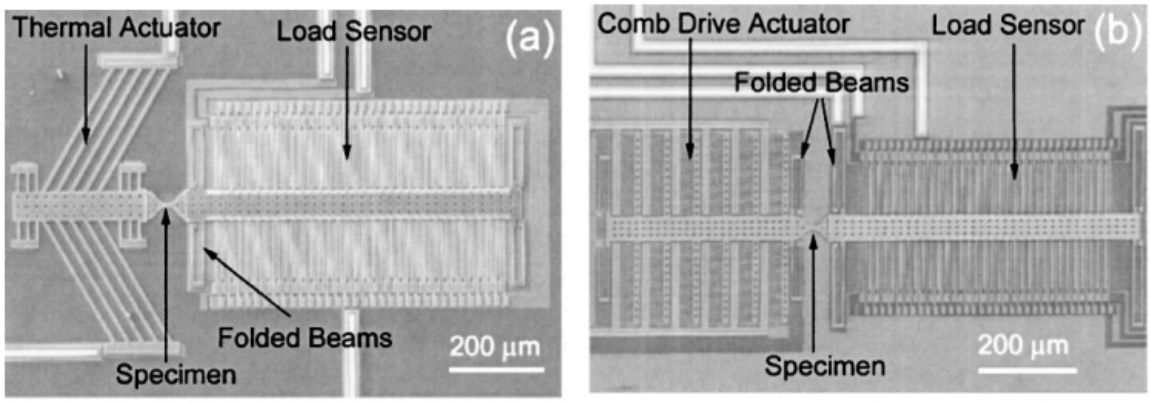

Figure 2.9: (a) Tensile testing device having a thermal actuator, load sensor and specimen [27] (b) Tensile testing device having a comb drive actuator, load sensor and specimen. [27].

nm in diameter [31]. The general trend observed reveals that at lower diameters, the strain to failure and associated strengths increase.

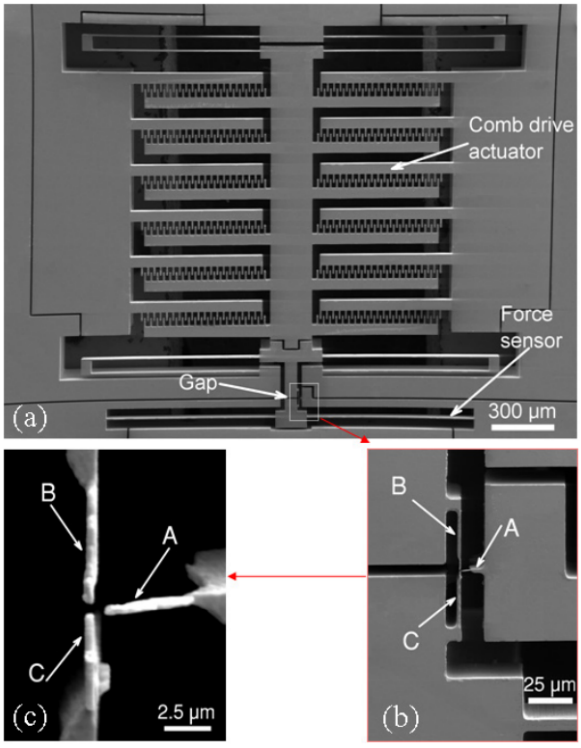

Figure 2.10: (a) SEM image of on-chip tensile testing platform having a comb drive actuator and a folded beam as a load sensor. (b) and (c) are close-up images pf the three-beam structure for the extraction of load and displacement information. [32]

Zhang *et al* performed a *in situ* uniaxial tensile loading on individual cobalt nanowires inside a scanning electron microscope [32]. The testing stage is a MEMS device consisting of comb drive actuator and a load sensor in the form of a folded beam (see figure 2.10). In order to simultaneously extract the load and displacement information from the device in the SEM, a "three-beam structure" was fabricated on the stage using focused ion beam induces deposition (FIBID). A similar platform was used to investigate the nonlinear elastic behaviour of palladium nano-whiskers with approximate diameter between 30 and 110nm by **Chen *et al*** [33].

2.1.4 Lab-on-chip devices

The deposition of thin films on a substrate is almost always associated with some level of internal stress. The nature and amount of internal stress present it the thin film thus induces some undesired effects in the film and/or substrate such as fracture, film delamination, buckling, microstructure evolution and crack initiation in the substrate. Depending on the origin of the internal stresses, they are classified as thermal, growth and epitaxial stress. The idea of the lab-on-chip devices for nanomechanical testing is thus to leverage on the internal stress present in the thin film during deposition to deform another film.

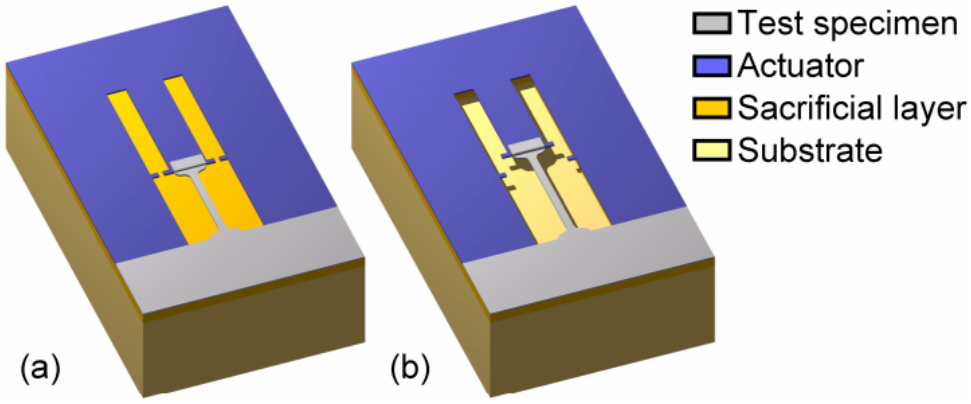

Figure 2.11: Lab-on-chip device for tensile testing of thin film structures.[34]

As show in figure 2.11 the on-chip devices consist of an actuator and the sample part both deposited on a sacrificial layer. When the set up is released, that is, etching of the sacrificial layer, the internal stress in the actuator material is allowed to express itself which pulls on the sample. The stress and strain of the sample is measured thanks

to the measurement of the distance of a moving and a fixed cursor once the set-up is released and from the knowledge of the Young's modulus of the actuator and the mismatch strain of both the actuator and the test specimen. In order to have the full stress-strain curve of the desired test specimen, several specimen of varying length is patterned on the substrate to obtain different points on the stress-stain curve (see figure 2.12).

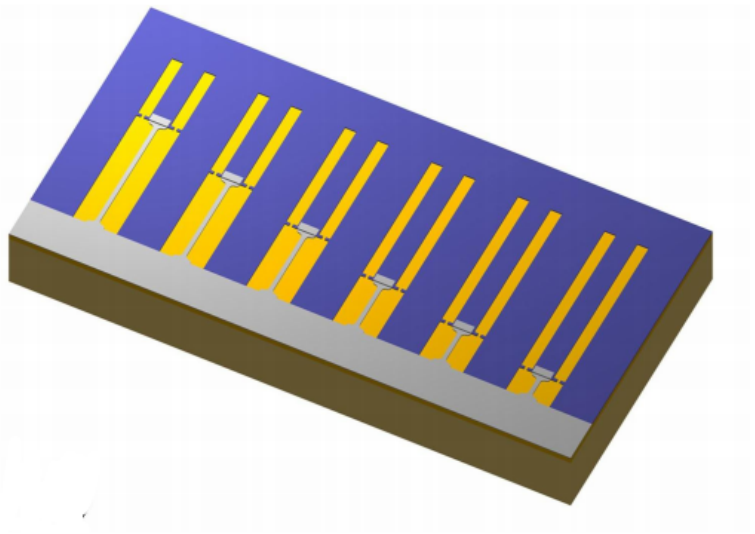

Figure 2.12: Lab-on-chip device showing tensile test with increasing gauge length from left to right.[34]

The actuator material is selected such that it contains a high level of tensile internal stress, as small as possible stress gradient in the thickness direction to prevent out-of-plane deformation, a high fracture stress, a linear elastic behaviour and a reproducible Young's modulus. The specimen may contain tensile or compressive internal stress which must be measured for the mechanical analysis. The lab-on chip device consist of {100} monocrystalline silicon wafers as substrate, a sacrificial layer of silicon oxide deposited by plasma enhance chemical vapor deposition (PECVD) and a silicon nitride actuator layer deposited by low pressure chemical vapor deposition (LPCVD). The desired geometry of the set is patterned using classical photolithography technique. The tensile testing stage have used to investigated the mechanical behaviour of palladium thin films deposited by electron-beam evaporation of 80, 160 and 310 nm [35, 36, 37] and aluminum thin films [38]. The same principle as above was used to perform uniaxial loading on an ultra thin (63 nm) passivated copper thin film [39].

2.2 Sample positioning

An important step in the mechanical testing of nanoscale samples is the positioning of the specimen at specific locations. A high throughput at nanometer resolution is also essential for this step. An additional criteria is that the specimen must be freestanding, lined up along the loading direction and fixed at both ends. The positioning of the sample can be achieve by nano-manipulation via the "pick-and-place" [28] and dielectrophoresis [40] method as well as co-fabricating the specimen with the testing device. In the following section, the different sample preparation methods are reviewed.

2.2.1 Pick-and-place method

This method of fixing test samples on MEMS devices was first introduced by **Zhu and Epinosa** [28] for the mounting of the palladium nanowires that were fabricated from templates of porous alumina templates [41]. The mounting process was carried out in four step. Firstly, ultraosnication was used to disperse the nanowires in isopropanol. Secondly, the dispersed nanowires were then deposited the grid of a TEM using a micropipette. The nanowires protruding from the grid edge were then manipulated and mounted between the actuator and the load sensor as the third and fourth step. The manipulation and mounting of the nanowires were carried out in the SEM/FIB equipment and summarized in figure 2.13. In essence it can be said that the "pick-and-place" method employs a nanomanipulator for the picking and transfer of a desired sample to a preferred location inside the SEM or a dual-beam (SEM/FIB) instrument while using a platinum precursor gas for the clamping of the sample to the MEMS device.

Although this method has been reported to manipulate sub-micron sized "dog-bone" shaped samples under a light microscope [42] and a wide range of other nanostructures [20, 32, 43, 44, 45, 46, 47], it nonetheless suffers from some drawbacks. The process step alone is tasking bearing in mind that it is and additional step to the process steps that may have been employed for the fabrication of the MEMS testing device and sample in the first instance. There is also the risk of sample contamination of the sample surface with the use of platinum precursor gas for clamping of the sample to the MEMS device. This could be a source of artifact when analysing the result of the tensile test experiment. Furthermore, it is also a concern if the clamping is strong enough and repeatable. Indeed, epoxy based adhesives have been used to clamp gold nanobeams [42] carbon nanotubes [48] in order to address the issues with the use of EBID which

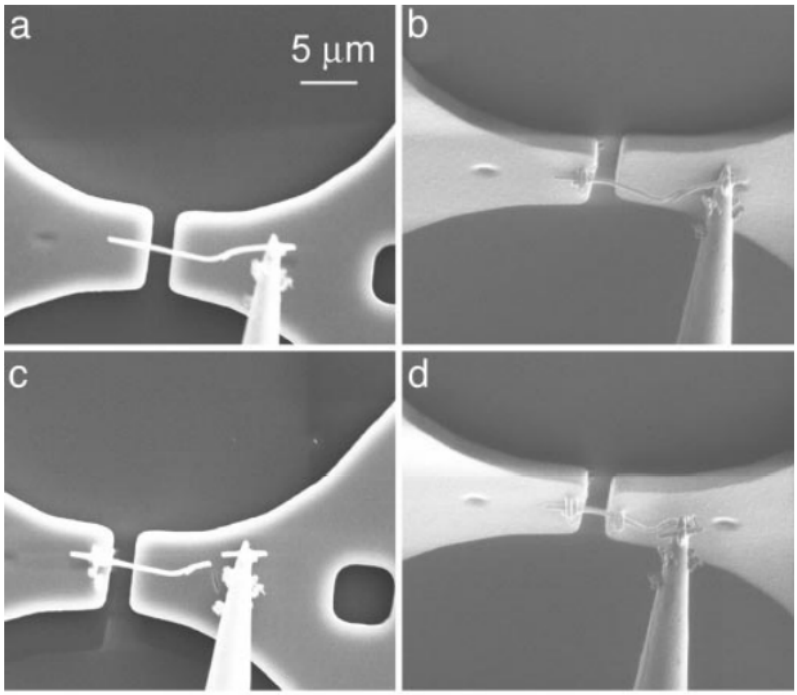

Figure 2.13: Procedure for the manipulation of Pd nanowires onto a MEMS device. (a) Bring the nanowire in contact with the MEMS device. (b) Pt gas is used to weld one end of the nanowire to the actuator shuttle using EBID (c) FIB is used to cut the other end of the nanowire (d) the free end of the nanowire is welded to the load shuttle after ensuring contact between the nanowire and the MEMS device by using the nanomanipulator to push on the nanowire. [28]

shows to be more practical and mechanically compliant [49]. The only challenge is the undesired charging issues during electron microscopy which limits their usage to the manipulation of relatively large specimen size in air under an optical microscope. Regardless of these drawbacks, the "pick-and-place" method of sample mounting is increasing in popularity because of the high level of flexibility offered.

In order to address the challenge with the transfer and mounting of specimen unto a MEMS device, **Liebig *et al*** [49] proposed a sample preparation method where the manipulation is not done directly on the sample as show in figure 2.14.

The goal is to ensure that the platinum clamping is kept far from the sample area and as such eliminate the potential of sample surface contamination. In order to fabricate this structure, the authors started by depositing silicon nitiride (SiN_x) layer (30-80nm) on a single crystalline silicon substrate. This serves as barrier to diffusion and prevents reaction between the material of interest and the silicon substrate. The material to be

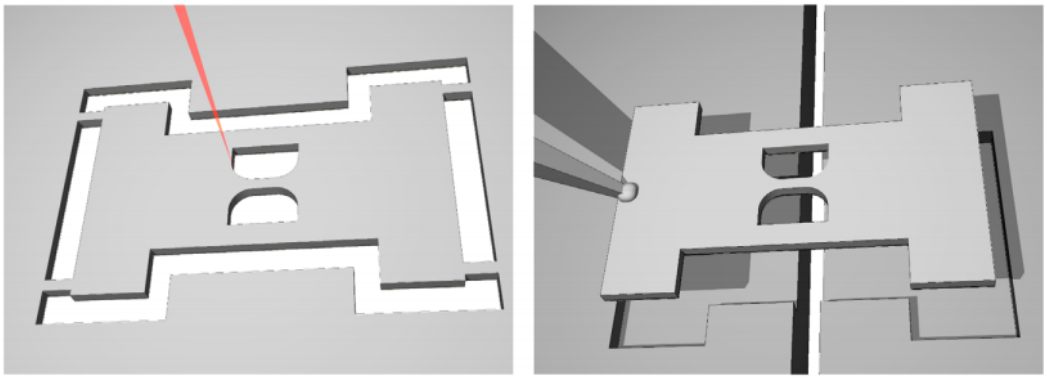

Figure 2.14: Schematic diagram of structure prepared by FIB milling to be transferred to a push-to-pull for *in-situ* tensile testing. The sample area is the dog-bone shape in the middle of the structure. [49]

investigated is thereafter deposited on the SiN_x layer. The substrate is then flipped over and milled using FIB in what is termed a shadow geometry to have the desired structure in figure 2.14. It is called shadow geometry because the silicon layer serves as a mask preventing the structure of interest from direct exposure to highly energetic ion beams. This structure is then transferred using a micromanipulator onto the testing device within the microscope. This way, the sample area is prevented from platinum contamination.

The final step is to locally etch the silicon layer on top of the sample of interest in the dog-bone area of the prepared structure as shown in figure 2.15. This is done by using selective electron-beam assisted etching. To achieve this, xenon diflouride (XeF_2) is locally immersed on the on the sample area using a gas injection system while scanning the area to etched with an electron beam. The procedure described above was used to prepare 50nm electron beam evaporated gold 80nm sputtered Cu-Al (5 at% AL) for *in situ* tensile testing in TEM. Some advantages of this process of sample preparation and positioning are listed below.

- The process is highly flexible in that specific geometries and area of interest can be cut using FIB milling since there is no mask required for the process as in the case of optical lithography.
- The silicon substrate serves as a support preventing the buckling of the sample.
- As mentioned earlier, the sample contamination associated with EBID platinum deposition is avoided.

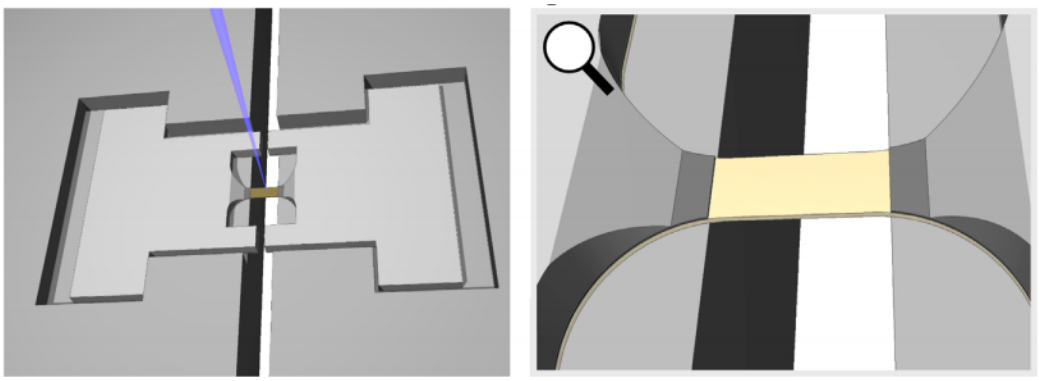

Figure 2.15: Schematic diagram of structure selective electron-beam-assisted etching of the silicon on top of the sample of interest. [49]

- The testing stage can also be reused after the tensile test.

Nevertheless, this method suffers some drawbacks especially with the use of FIB for the milling of the sample. There is the possibility of liquid metal embrittlement in the case of aluminum [50] due to the formation of gallium residue on the substrate side of the free standing thin film. The is also the potential for the re-deposition of sputtered materials onto the area of interest which may be a source of artifacts. Lastly, the process is time consuming when compared to lithography method of sample preparation where numerous samples can be printed simultaneously.

2.2.2 Dielectrophoresis method

Dielectrophoresis essentially means the exertion of a force on a dielectric particle by subjecting it to a non-uniform electric field. It is not required that the particle is charged for the exertion of the force. The strength of the force however depends on the electrical properties of the particle, its shape and size as well as the electrical field frequency. As such, particles can be manipulated based on the frequency of the electric field [51]. **Lu *et al*** used this method to suspend "templated carbon nanotubes" (T-CNTs) across two opposing electrodes having a 100 µm deep trench in-between them as shown in figure 2.16 [40].

The deposition of the T-CNT was achieved by using electric field guided method with the T-CNT dispersed in ethanol and the structure in figure 2.16 placed in a reservoir enclosing the electrode pair. Just before the evaporation of the ethanol, the sample was placed in beaker filled with 15 ml of 100% ethanol and then placed in the critical drying

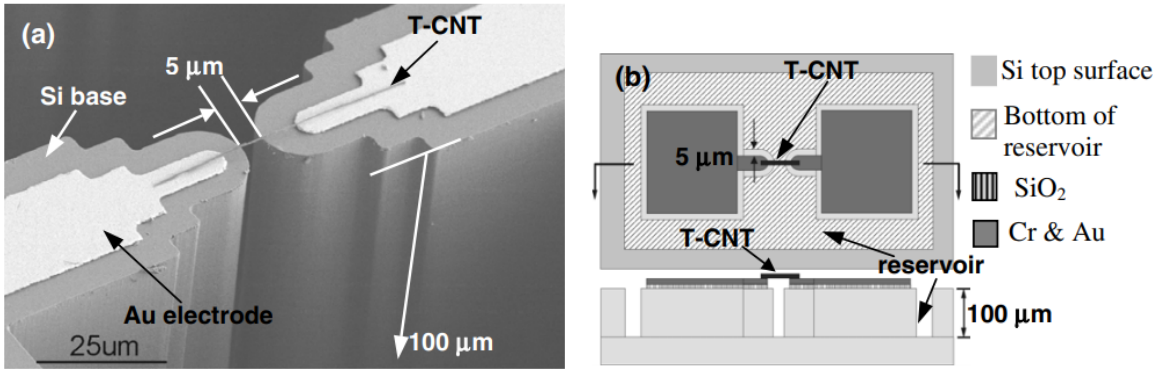

Figure 2.16: (a) SEM image of the mounted T-CNT across opposing electrodes [40] (b) schematic diagram of the top and side view of the structure. [40].

point instrument. Otherwise the ethanol will evaporate and the dispersed T-CNTs will form bundles and they could also be deformed in the process. Prior to the tensile testing of the mounted sample, the ends of the T-CNT was welded to the electrodes using EBID. Meanwhile the electrode structure was made by microfabrication process with the trench obtained by deep reactive ion etching (DRIE). Dielectrophoresis has also been used to mount gallium nitride nanowires unto MEMS device [18]. This method is more scalable when compared to the "pick-and-place" method only that the it has a low yield and the process is prone to contamination [12].

2.2.3 Co-fabrication method

Another method of "mounting" the test specimen is by totally avoiding the need to manipulate the sample by co-fabricating it with the MEMS testing device. In essence the specimen is fabricated alongside the load sensor and/or the actuator. In the pioneering work of **Haque and Saif**, the co-fabrication was achieved using lithography and micro-machining technique [26] summarized in **Appendix A.1**. An interesting feature of the tensile test chip is its capability to detect and measure the tensile internal stress present in any pre-stressed specimen by reading the displacement of the force sensor (see figure 2.8). It is noteworthy that the fabrication process employed delivered a flat specimen which could either imply that the specimen is unstressed on is subjected to tensile internal stress. Meanwhile, the test device was designed to be used in a TEM with a straining stage. More on that in **section ??**. This technique of nanoscale tensile testing of thin film have been used for *in situ* TEM testing of 100nm thick [52] and 30-50nm thick [53] aluminum thin film. Even though the method of sample mount-

ing provides perfect alignment and gripping, there is however a high chance of sample failure and the force sensor can only be calibrated after the sample testing [54].

A similar testing stage was also reported by **Han and Saif**. The modification in this case is that the displacement gauges are close to each other [54]. The new stage prevented the issue with sample failure mention earlier and also allows for the calibration of the force sensor before the sample testing. In addition to the measurement of the stress and strain of the sample of interest, the device can also be used to measure the electrical resistivity of the sample at different temperatures. Futhermore; the fabrication of the device requires only two optical patterning and a single silicon etching step.

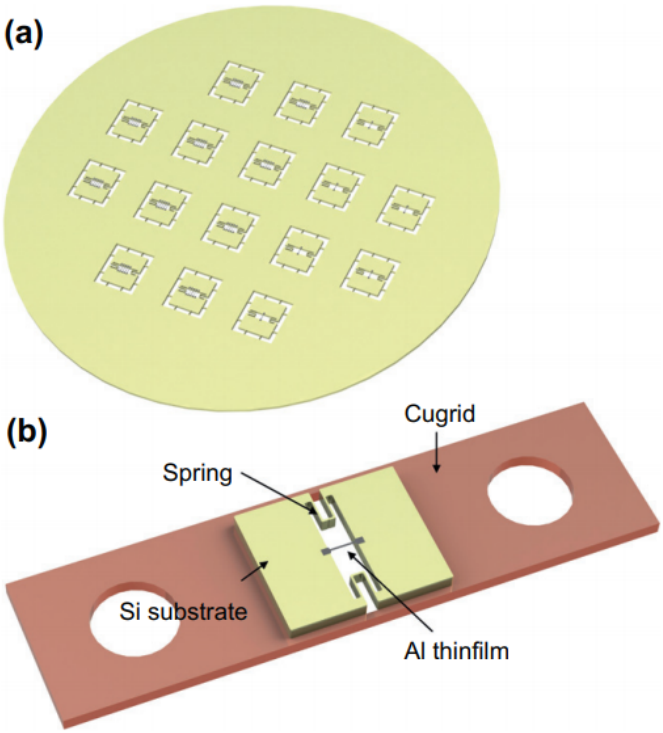

Figure 2.17: (a) An area of testing device on silicon wafer (b) One of the testing device glued on a copper grid for *in situ* tensile testing in TEM. [55]

The idea of co-fabricating the sample with the MEMS device was also employed by **Mompiou *et al*** to investigate the plasticity mechanism in aluminium thin films [55] as shown in figure 2.17. Evaporation technique at room temperature was used to deposit 300nm thick pure aluminum on a silicon substrate having a 1µm thick SiO_2 layer. The dog-bone shaped tensile specimen was then patterned using photholithography and dry

etching. A modified Bosch process was then used to etch the silicon substrate from the back in order to have a window for the TEM viewing. Finally, the sacrificial layer was then etched with hydrofluoric acid (HF) accompanied by rinsing in isopropanol (IPA) in order to have a free standing specimen. The U-spring-shaped feature on the sides of the device allows for easy manipulation which was otherwise difficult [56]. A procedure closely resembling the one described above have also been used to prepare polysilicon [57] and nanocystalline palladium [58] thin films for on-chip nanomechanical testing.

2.3 Mechanical straining in TEM

In more general term, the transmission electron microscopy technique uses beams of electrons transmitted through an ultrathin specimen to form an image at high resolution of about 0.2nm. The thickness of the specimen is usually required to be less than 100nm while the image formation is brought about by the interaction between the electrons and the sample during the transmission through the sample. In essence, a typical TEM column consists of an electron source for the generation of the electron, an electromagnetic lens system to have medium to high energetic electrons reaching the specimen in the sample holder while the result is obtained from the imaging system (see figure 2.18).

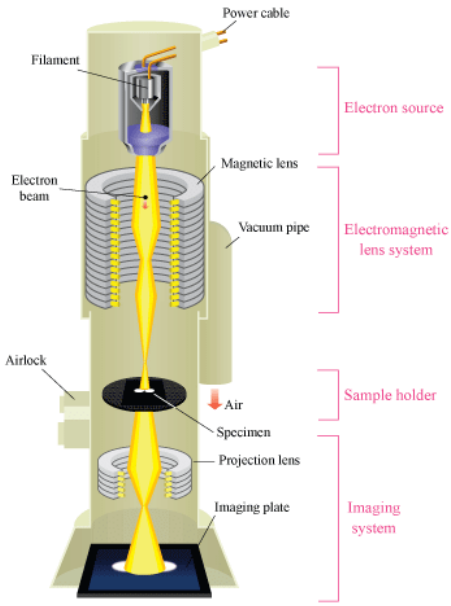

Figure 2.18: Schematic diagram of the components of a transmission electron microscope. [59]

In the context of this work, applying and measuring in the TEM is crucial for *in situ* mechanical testing and various approaches have been adopted. This could simply rely on the used of TEM holders for mechanical actuation or fabrication of MEMS devices consisting of actuators and load sensors as described in section 2.1.2 and 2.1.3. In addition, the difference in thermal expansion co-efficient of materials can also be used to achieve straining which is a key feature of the lab-on-chip devices (see section 2.1.4). In this section, the use of TEM holders for mechanical straining at nano-scale will be reviewed.

The basic straining holders used in the TEM are the classical tensile holders. The operating principle is shown in figure 2.20. The ultra thin sample is prepared and glued to a deformable grid which is fixed to the tensile holder. Straining is achieved thanks to the long rigid shaft driven by a worm gear box powered by electric motors. A straining speed ranging between 10 nm/s and 10 µm/s can be achieved with this simple set-up [60]. The use of this kind of straining technique have been reported in literature [26, 55].

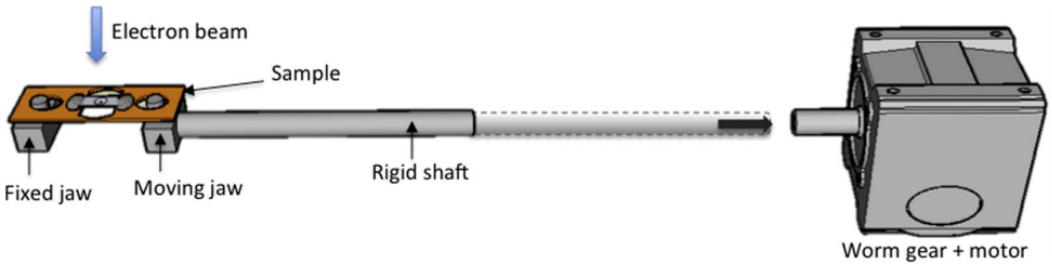

Figure 2.19: Operating principle of standard straining holders in TEM. [60]

An advantage of the classical TEM holders is its simplicity and versatility. Once the thin film are properly prepared and glued to the grid, they can be strained immediately [61]. Heating and cooling can also be added to this type of holders. A miniaturized furnaces or lasers can be used for heating the sample if needed [62]. The drawback with the use of classical TEM holder is that only the displacement of the sample of interest can be measure. Other variants of this kind of holder for tilt straining [63] and bending [64] can also be found in literature. A New generation TEM holders like the PI-95 picoindenters [65] are equipped with load cells to which provides the capacity for load measurements.

Figure 2.20: PI-95 picoindenter. [65]

2.4 State of the art: general conclusion

In the previous section, a number of nano-mechanical testing methods have been briefly presented with more emphasis on tensile testing at nano-scale. The techniques considered have been grouped into three broad classes namely; *(i)* those that those that do not have a direct load sensor, *(ii)* those that have a direct load sensor and *(ii)* a complete testing system that has both load senor and an on-chip actuator. Although the third class of nano-testing device configuration mirrors what is macroscopically obtainable, it often relies on specific fabrication procedure. A novel method using the presence of internal stress in thin film for mechanical straining of materials of interest have also been considered. This method is however limited when incorporating it with in-situ tensile testing.

Although a wide range of nano-structured materials have been studied extensively, there is limited report the tensile properties of thin films below 50nm. This can be attributed to the complexities with the fabrication and manipulation of such tiny and fragile structure. This thesis therefore aims at fabricating a rigid frame that will ensure the easy manipulation and transfer of thin film structures below 50nm thickness. The aim is to be able to perform in-situ tensile test on such structure using the push-to-pull device in the TEM.

Chapter 3

Experimental Method

As mentioned earlier, the goal of this thesis is to fabricate a metallic frame that will facilitate the manipulation and transfer of thin film structures that are thinner than 50nm onto a tensile testing platform like the push-to-pull for in-situ tensile investigation in the TEM. This is also clear from the review of literature that there still exit a gap with the *in-situ* tensile testing of thin films below 50nm thickness. The success of such endeavour will indeed give more insight into the understanding of the deformation behaviour materials as well as open further research question for thin film materials. In the following section, the preparation of a frame along with a free standing tensile specimen is described. The focus is specifically to prepare specimen for *in-situ* tensile testing in TEM with the aim of addressing the challenge with sample transfer and mounting.

3.1 Frame design concept and specification

The inspiration for using metallic frame for the transfer of ultra thin film tensile specimen is drawn from the work of **Liebig *et al*** [49]. Although the method they employed was highly flexible, it suffers a major drawback due to the potential damage that the use of FIB for sample machining could have on the quality of the sample. Due to the high energetic gallium ions used for FIB milling (around 30KeV), this could cause surface diffusion and a local rearrangement of atoms [66, 67, 68] hence, the result of the tensile testing may not be representative of the actual sample. More so there is also the trapping of gallium atoms in the surface up to 10% of the specimen [69].

The aforementioned drawbacks thus requires the use of a novel sample preparation that will mitigate the negative effects associated with FIB machining. An alternate method would be to use lithography based techniques for the sample preparation which is known to produce pristine structures [42, 70, 55]. They may however be limited in terms of flexible due to the need for photomasks and the requirement of multiple process steps. In the framework of this thesis work, a two-step photolithography process have been employed for both the fabrication of the frame and the tensile sample. This will be detailed in section 3.2.

The frame is in essence a square section having a tensile sample in the middle. It's main purpose is to hold the tensile sample in place during the manipulation as well prevent the sample from contamination due to welding by EBID. A key requirement for the frame is then to posses a high stiffness and low internal stress at sub-micron thickness. For this reason, aluminum has been chosen as the material for the frame as it is a well known clean room material.

The conceptual designs that were arrived at for the frame-sample structure are shown in figure 3.1. The first design consideration is to ensure that the aluminum frame can bear the weight of the tensile specimen without damping. It was therefore considered that the aluminum frame is sufficiently thick for this purpose. As such, the thickness of the aluminum frame was set at 300 nm since which is approximately ten times the thickness of the sample (about 30 nm). Furthermore, the number of anchors holding the aluminum frame in place was initially thought to vary between 1 and 4. However, more anchors would require more FIB cutting steps of the anchors. This would of course require more time and poses more risk of sample contamination. The different variants of the number and type of anchors are shown in figure 3.1 which only vary between 1 and 2 anchors.

Another source of sample contamination will be during the welding of the frame-sample structure unto the push-to-pull device for tensile testing. Indeed IBID will be used to perform the welding of the frame and not the sample along the edges of the frame. This idea is expected to reduce the risk of sample contamination from the welding process. Moreso, the sample is kept at a considerable distance from the edges of the aluminum frame. Thus the frame is set to be 16 µm in length and breadth while varying the width of the frame between 2 and 4 µm. Thus the gauge length of the tensile sample for the different frame structures varies between 4 and 8 µm. This is sufficient to run over the gap of the push to pull ($\sim 2.5\mu m$) as the dimensions of the frame are also limited

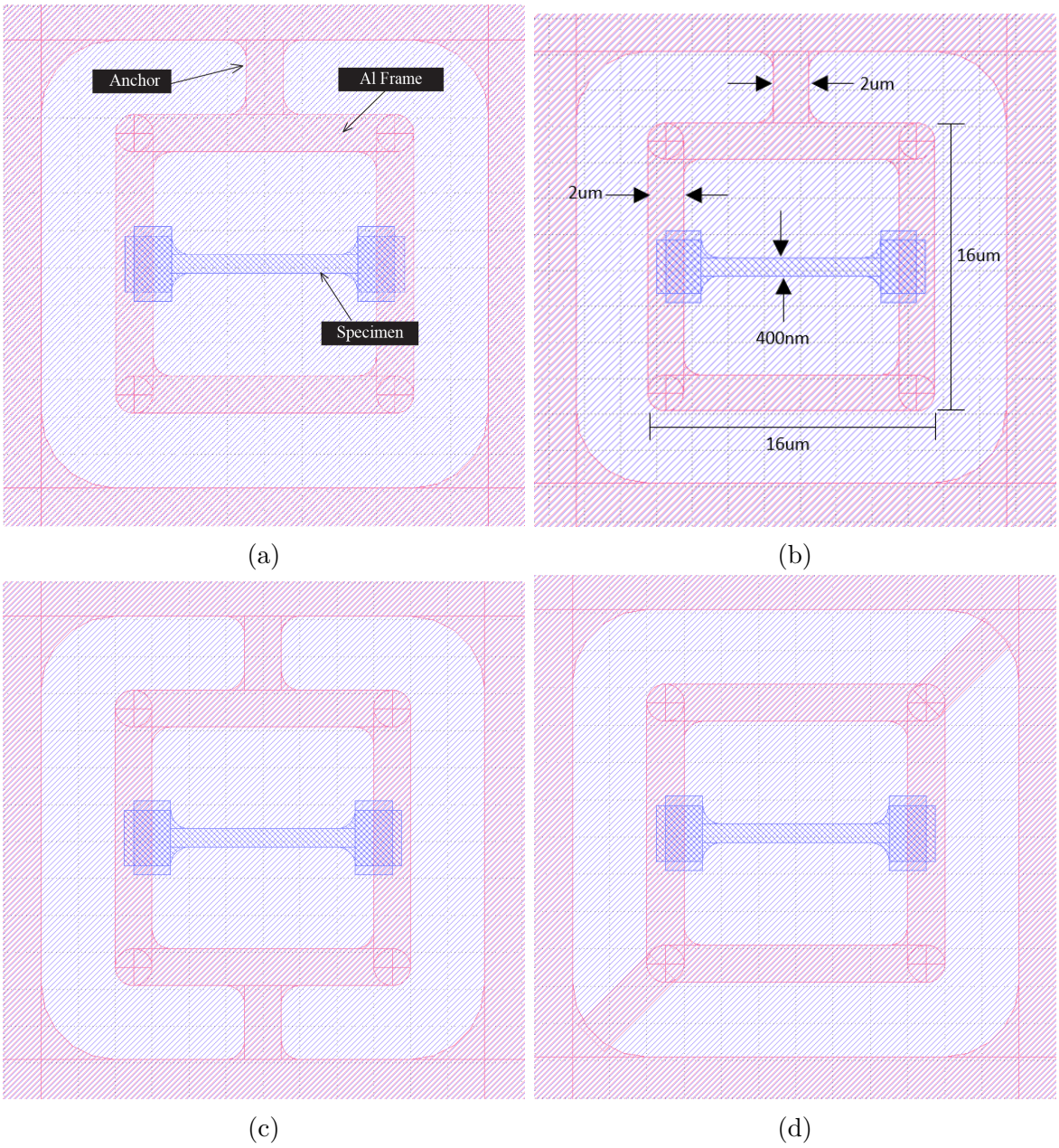

Figure 3.1: Conceptual designs of aluminum frames having a specimen in the middle showing (a) the different components of the entire structure, (b) the dimension of the frame and sample; and other variants of the frame having (c) two anchors perpendicular to the long direction of the sample (d) two anchors at connecting the corners of the frame to the grid.

by the dimension of the PTP. The maximum allowable dimension with respect to the PTP is 20 microns. Furthermore, the width of the test specimen was varied between

400 nm to 1 µm with an increment of 100 nm. The goal of this is to experiment the use of photolithogrpahy to achieve "sub-micronic" structures. Indeed, the best method to print sub-micronic structures unto a silicon substrate is e-beam lithography. The different variants of the frame as well as other test structures that have been designed alongside the frame are shown in Appendix B.2.

3.2 Fabrication process

The fabrication process for the frame-specimen structure involves a total of eight (8) steps that are summarized in figure 3.2. One can name it a "two-step" photolithography process as the entire fabrication process revolves around two photolithography steps. Indeed the second photolithography step is a critical step. Care must be taken at this stage to have a proper alignment of the frame on the sample. The sections after this will give more details on each fabrication step.

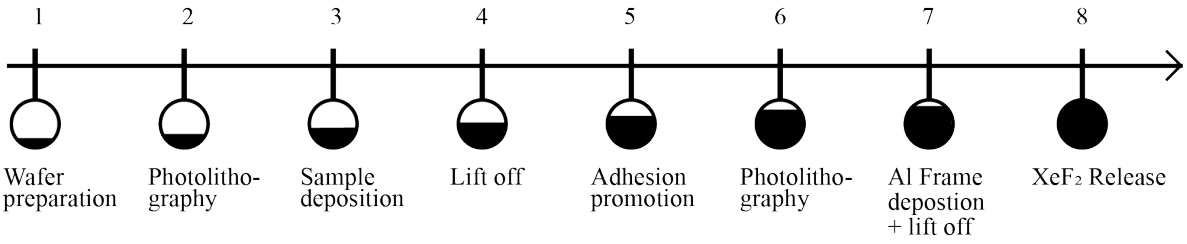

Figure 3.2: General overview of the fabrication steps for the frame-sample structure.

3.2.1 Step 1 - Silicon wafer surface preparation

The fabrication process starts with the standard cleaning of the silicon wafer in other to remove the native oxide and organic contaminants from the wafer. The process is standardized and carried out at one of the wet benches of the WinFab facility of UCLouvain in order to ensure repeatability. First, the wafers were dipped in a "Piranha" bath which is a mixture of H_2SO_4 and H_2O_2 at 100^{o}C for 10 minutes. This is then rinsed in demineralized water with a usual practice of allowing an inlet of water from the bottom of the bath until all the silicon wafer is covered and then releasing the water. This is done five (5) times and then leaving the silicon wafers in the demineralized water until a total time of 10 minutes for rinsing is achieved. The process of dipping in a "Piranha" bath and rinsing in demineralized water is repeated a second time while also pumping nitrogen gas into the demineralized water during the second rinsing. These two steps are to remove all organic contaminants that may be on top of the silicon

wafer. The last step of the standard cleaning which removes the native oxide on the silicon is to dip the wafers into a solution of 2% HF for 15 seconds. In order to check if the native oxide has been stripped off the wafer, it is expected that the surface of the silicon wafer remains hydrophobic otherwise process is not successful and has to be repeated. The wafers are thereafter immediately stored in water and transported to rinser-dryer machine, a process step that takes approximately 8 minutes and a working speed of 2000 rpm.

Furthermore, the wafers were then carefully placed in the degassing oven at 800^oC for 20 minutes to ensure that silicon wafer surface is completely dry otherwise there would be a loss of resolution and/or adhesion during the resist coating step. These are then immediately transferred into the LPIII oven for resist adhesion promotion by applying hexamethyl disilazane (HMDS) vapor at reduced pressure on the wafer for a period of 23 minutes. This forms a monolayer of silane on the wafer that prevents water readsorption. It is important to note that the steps described above has to run one after the other without a delay or pause in between each step otherwise the native oxide layer on the silicon will be formed and the process is defeated.

3.2.2 Step 2 - Photolithography

Photolithography otherwise termed optical lithography or UV lithography is a technique that uses UV light to transfer a pattern on a photomask unto a substrate. Essentially, the photomask exposes certain parts of a photoresist on the substrate to the UV light thanks to the chromium pattern drawn on the photomask. The major advantage of optical lithography is that a lot of patterns can be drawn at once and as such it less time consuming when compare to electron beam lithography although e-beam lithography provides a better resolution.

Photoresist spin coating

Spin coating is a standard process of obtaining a continuous thin film of photoresist on a silicon wafer. To achieve this, a few drop of photoresist is applied on a slowly rotating wafer before ramping up the speed as required. In this specific case, a negative photoresist (Nlof 5510) was used at a rotating speed of 3000 rpm to obtain a resist thickness of 1µm. The thickness of the resist actually depends on the rotating speed, acceleration and resist viscosity and can be obtained from the manufacturers manual for specific photoresist. The resist coating is automated using the SUSS Gamma equipment in the WinFab facility at UCLouvain. It is also a usual practice to ensure that formation

of bubbles during the application of the resist is avoided. This is to ensure that the resist spin coating is uniform and continuous.

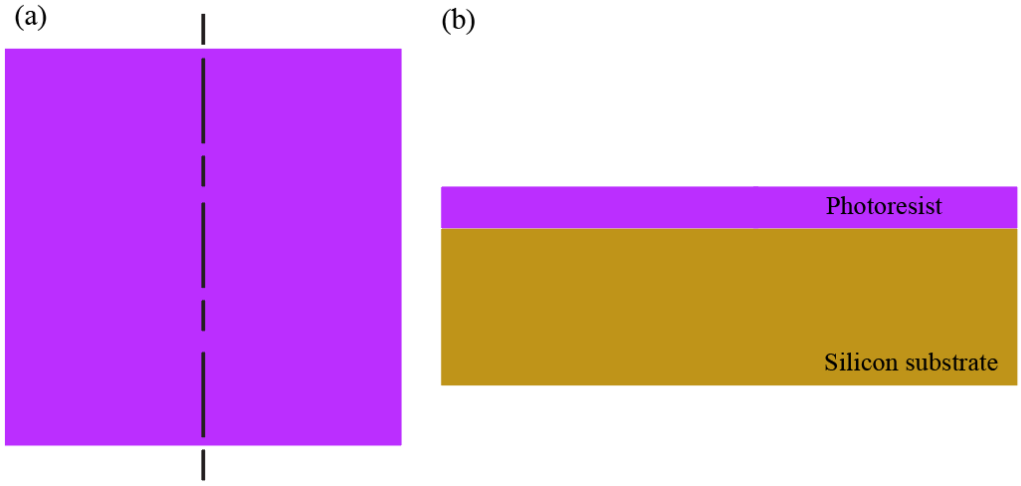

Figure 3.3: Schematic diagram of (a) top view and (b) cross-sectional view of the substrate after resist coating.

Pre-exposure bake

The three main components of the photoresist are *(i)* base resin for mechanical stability and thermal properties, *(ii)* photactive compound for resist sensitivity control and *(iii)* solvent for viscosity control. The goal of this step is therefore to remove the solvent present in the resist. Care must however be taken in order to avoid decomposition of the photoactive compound which can have a negative consequence on the sensitivity and resolution of the resist. In this specific case, the wafers were placed in the oven at 90^oC for 60 seconds.

Exposure

At this step, the photoresist on the silicon wafer is exposed to UV light. This step was performed using the MA6 equipment at the WinFab facility of UCLouvain. In practice, the wafers are carefully placed on the sample holder and then held tightly by engaging the vacuum. A wedge compensation step is then initiated to ensure that the wafer and the mask are lying parallel to each other before the actual exposure to UV light. It is possible to carry out the exposure either using the proximity, soft contact or vacuum contact mode. The proximity mode brings the mask close to the substrate without contact, the soft contact mode ensures that the mask is in contact with the substrate while the vacuum contact mode employs both contact and pressure between the mask

and the substrate for maximum resolution. The vacuum contact mode was used in this present work with an exposure dose of $120mJ/cm^2$ at 1000 W.

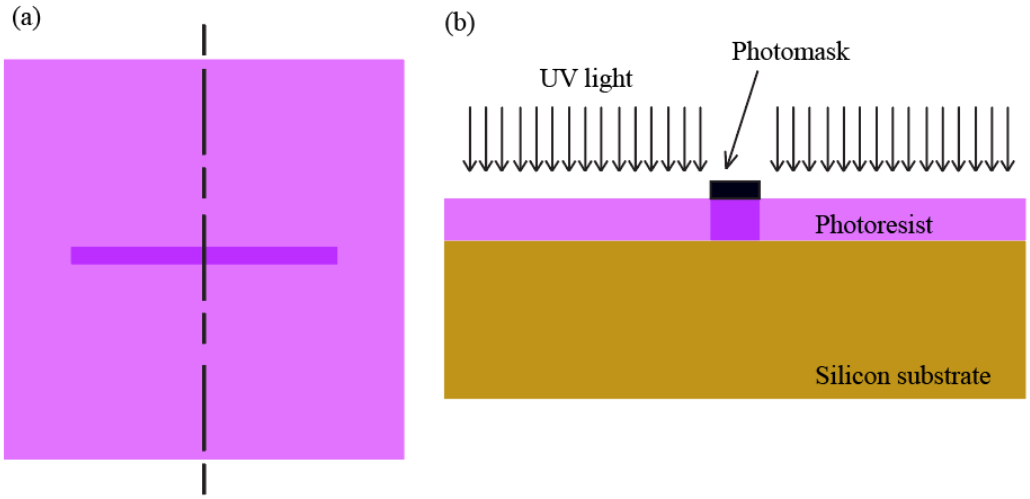

Figure 3.4: Schematic diagram of (a) top view and (b) cross-sectional view of the substrate after exposure.

Post exposure bake

The aim of the post exposure bake is to have an effect where there is a difference in the solubility between the exposed and unexposed part of the photoresist. This is achieved by placing the wafer in the oven at 105^oC for 60 seconds.

Development

Since a negative photoresist was used, the exposed part of the photoresist undergoes polymerization and thus becomes insoluble in a developer. The soluble part of the photoresist is then dissolved in a developer in order to have the pattern on the mask transferred to the substrate. 0.26M of tetramethyl ammonium hydroxide (TMAH) was used as the developer and the wafers were thereafter rinsed with water and dried to complete the development.

3.2.3 Step 3 - Sample deposition

The next process step after the photolithography is the deposition of the test specimen onto the substrate. Four materials were decided upon as demonstrators which include copper, aluminum, alumina and graphene. In fact any material that is is not etched by XeF_2 can be deposited as a demonstrator. This is because the final step to have a free standing test specimen involves silicon etching by XeF_2.

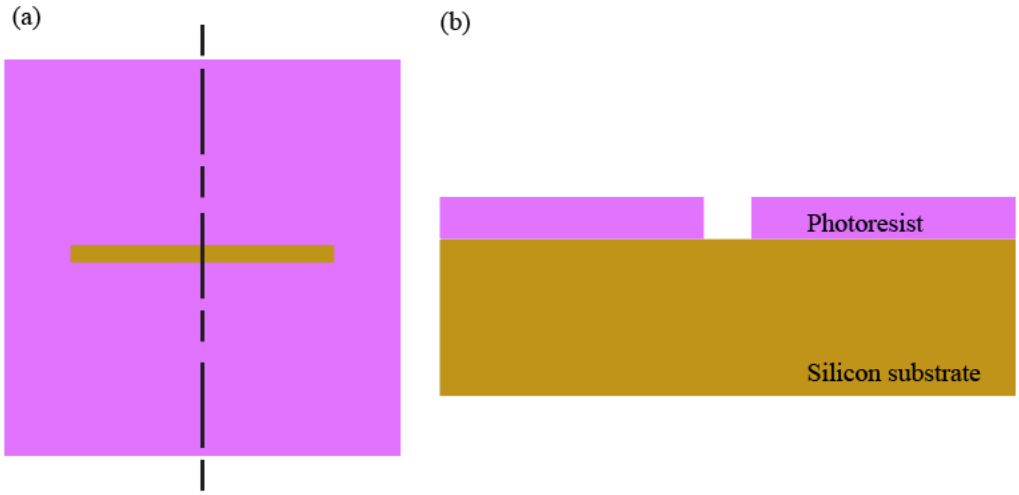

Figure 3.5: Schematic diagram of (a) top view and (b) cross-sectional view of the substrate after development.

Thin films are usually deposited either by chemical vapor deposition or physical vapor deposition. The later is more adaptable and environmentally cleaner since it does not require a combination of specific chemicals. In addition, physical methods produces structures with better adhesion and also requires lower temperature [71]. In fact all aluminum thin films are deposited using physical methods [72] with evaporation and sputtering being the most common. In this current work, the copper demonstrator was deposited evaporation while the aluminum and alumina demonstrators were deposited sputtering. The method for the graphene transfer will be detailed in section 3.3.

The Vacotec e-Gun double beam evaporator present in the WinFab facility at UCLouvain was used to perform the deposition of copper demonstrator. In principle, the metal to be deposited is placed in the evaporation source while heating is achieved either by resistive heating or electron beam gun (see figure 3.6). The deposition process is termed e-beam evaporation when the heating is achieved using an electron beam gun as in the case of the Vacotec machine. In essence, the copper is placed in the evaporation source and heated using electrons extracted from a tungsten filament. The electrons are accelerated at high voltage typically between 5 to 10kV and focused on the source material thanks to electrostatic lenses. During the metallization, the atoms from the source material hits the substrate maintaining a line-of-sight route without collision due to the ultra high vacuum of the system. A combination of low temperature deposition and line-of-sight transport during e-beam evaporation gives rise to a non-comformal

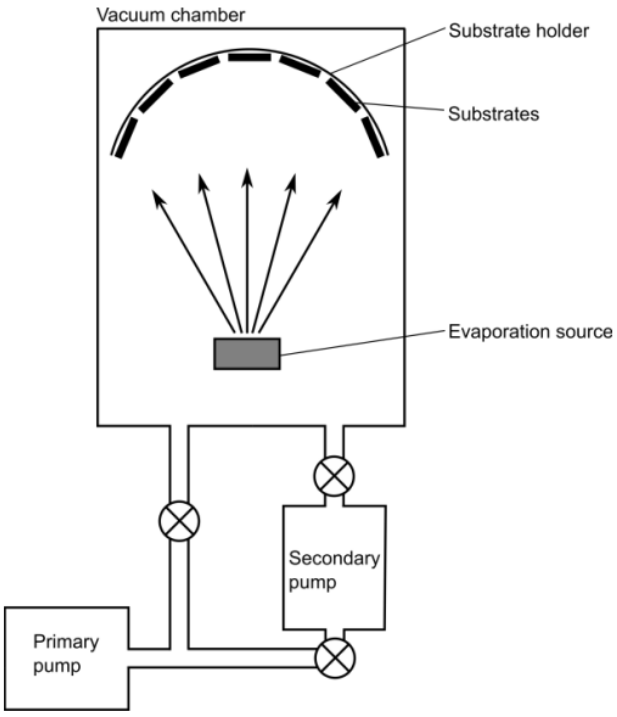

Figure 3.6: Schematic diagram of the e-beam evaporation system [73].

deposition. This means that holes, ridges and side walls are not well coated however, a good film quality is achieved on planar surface [72]. A non-comformal deposition is indeed a technical requirement for the next process step in section 3.2.4.

The aluminum and alumina demonstrators were deposited by sputtering, a technique that ejects atoms from a negatively biased target (material of interest) unto a substrate using argon ions form a glow discharge plasma see figure 3.7. The ejected atoms are transported at quite high pressure (1-10mtorr) unto the wafer in a vacuum at a deposition rate (1-10 nm/s) higher than that of evaporation (0.1-1 nm/s). Introducing oxygen into the sputtering atmosphere gives rise to the deposition of oxide thin films. The sputtering parameter using in this present work is summarized in Appendix A.2.

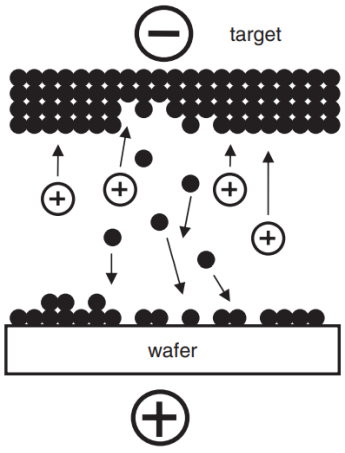

Figure 3.7: Graphical representation of the sputtering process. [72]

The sample deposition step gave rise to a thin film of approximately 30nm in thickness for the aluminum, alumina and copper demonstrators. This was confirmed using the profilometer and summarized in Appendix B.1.

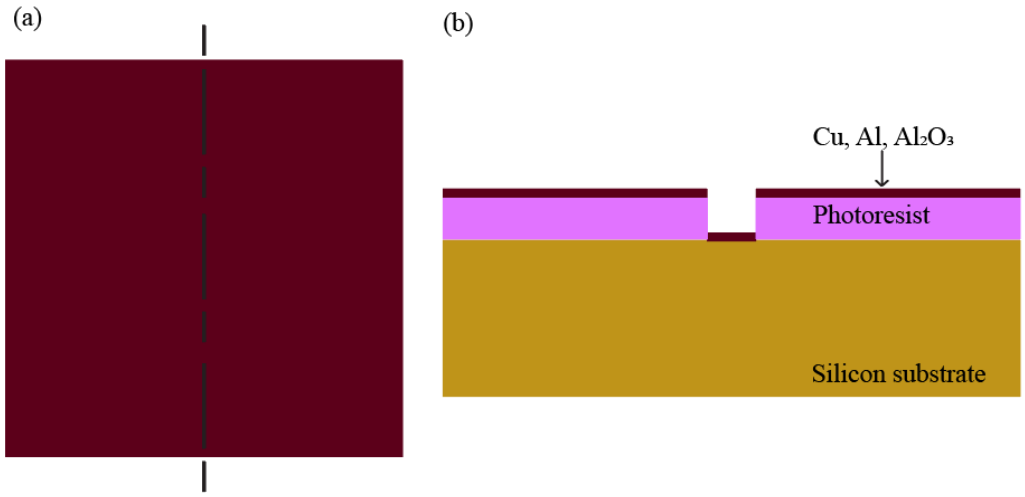

Figure 3.8: Schematic diagram of (a) top view and (b) cross-sectional view of the substrate after sample deposition.

In addition, a separate silicon wafer was prepared for the measurement of the internal stress present in the deposited thin film by Stoney measurement (see equation 3.1). In essence, the radius of curvature of the silicon substrate is measured before and after the thin film deposition then three (3) days after the deposition using the profilometer and the Stoney formula is used to determine the nature and magnitude of the internal stress present in the thin film.

$$\sigma_f = -\frac{1}{6}\frac{E_s}{1-V_s}\frac{{h_s}^2}{h_f}\left(\frac{1}{R}-\frac{1}{R_0}\right) \tag{3.1}$$

where σ_f = internal stress in the thin film,
E_s = Young modulus of the silicon substrate,
V_s = Piosson ratio of the silicon substrate,
h_s = thickness of the substrate,
h_f = thickness of the thin film,
R = Radius of curvature of the substrate after thin film deposition,

R_0 = Radius of curvature of the substrate before thin film deposition.

3.2.4 Step 4 - Lift off

The goal of this process is to etch the remaining photoresist present on the silicon substrate and as a consequence remove the unwanted thin film on the photoresist. To achieve this, the silicon substrates were placed in a beaker filled with acetone. The beaker is then placed in the **Elmasonic P** equipment at a frequency of 37 KHz and room temperature. A technical requirement is to ensure that the wafers are placed vertically during the lift off hence a wafer holder was used to dip the wafers into the acetone solution. It is also required that the thickness of the resist is require to be at least twice the thickness of the deposited sample. Otherwise, the lift off would be difficult to achieve. Once the liff-off is complete, the wafers are rinsed with acetone, methanol and water in succession and then dried with the nitrogen gun. In order to ensure that copper and alumina demonstrators are free of moisture as much as possible, they were placed in the main chamber of the Xactix equipment under vacuum for at least 30 minutes. This is to further enhance the adhesion of the photoresist that will be subsequently applied to the substrate during the second photolithography step. Optical images taken after the lift off step is shown in figure 3.9.

..

From figure 3.9d, it can be seen that the lift off for the aluminum demonstrator is incomplete even after almost an hour of lift off. This could be a result of the comformal deposition of the aluminum which was not the case for the alumina demonstrator as it appeared to show a complete lift off (see figure 3.9c). A solution would be to deposit the aluminum using e-beam evaporation as in the case of the copper demonstrator (see figure 3.9a and 3.9b).

3.2.5 Step 5 - Adhesion promotion

The next step after the specimen deposition and lift off is to deposit the aluminum frame on the specimen. An intermediate step is to perform adherence promotion before photo resist spin coating in order to have a good resolution. This is carried out in the LPIII oven as explained in section 3.2.1. This was only done for the alumina demonstrator in order to avoid the oxidation of copper due to the working temperature of the adherence

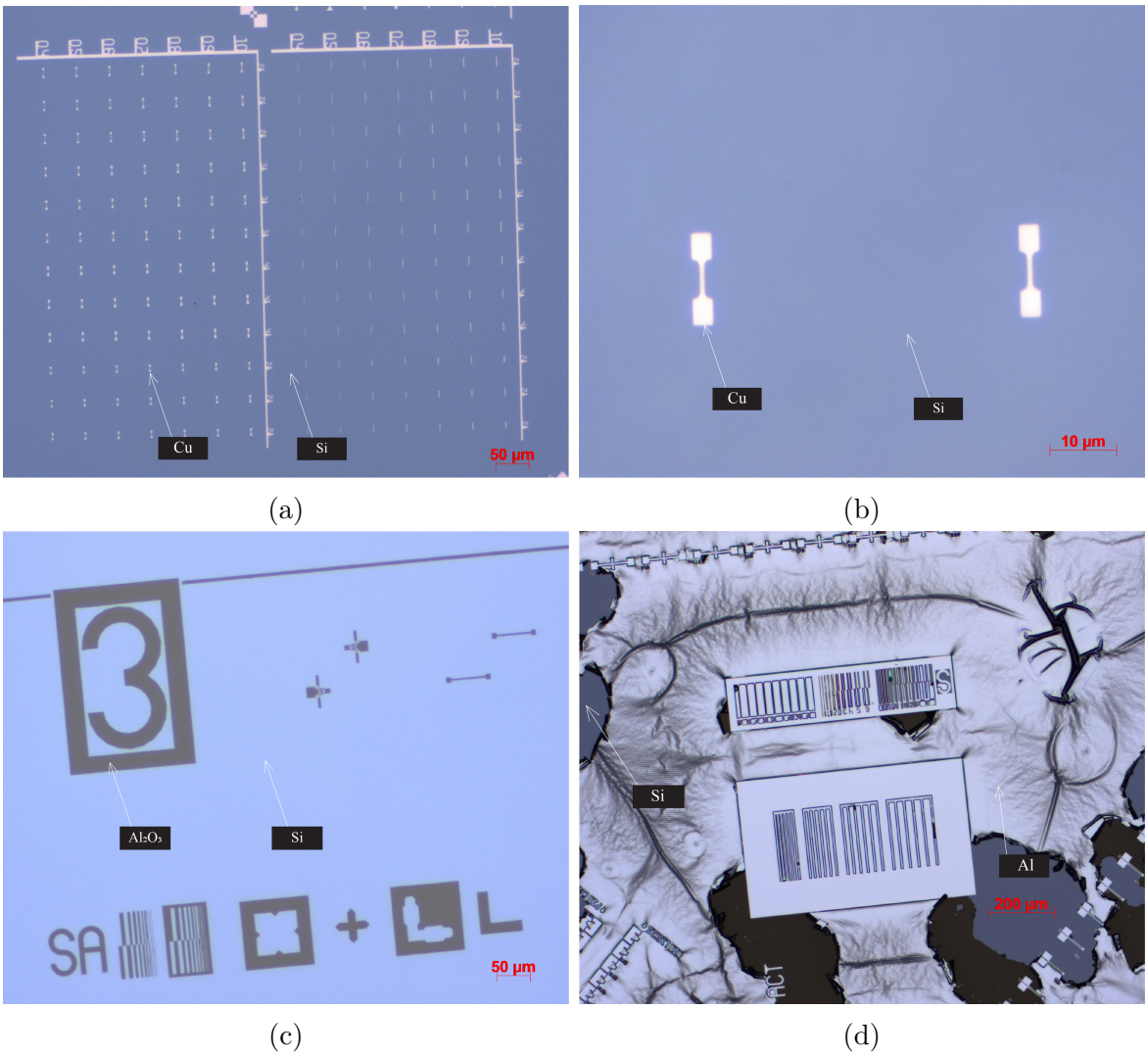

Figure 3.9: Optical microscope image of (a) an array of copper test specimens on a silicon substrate (b) a close-up view of one of the copper test specimen (c) alumina on silicon substrate and (d) aluminum on silicon substrate after the lift off step.

promotion step.

3.2.6 Step 6 - Photolithography with mask alignment

The second photolithography was carried out following the same procedure as outlined in section 3.2.2. The only exception was that a different negative photoresist (Nlof 2020) was spin coated at 3000 rpm to have a resist thickness of 2 µm. This was because a 300 nm thick thin film deposition of aluminum and a lift off step is planned afterwards. A critical procedure at this stage was the alignment of photomask of the aluminum frame

with the sample already deposited on the silicon substrate. This was painstakingly carried out manually and guided by the alignment marks on the mask and the silicon substrate. This step was however unsuccessful for the alumina demonstrator as it was impossible to view the alumina during the alignment step. A proposed solution is to deposit a separate metallic alignment mark before the alumina sample deposition. That way, it would be possible to perform the alignment on the metal and not the alumina. This would however mean a adding an additional step to the entire process with the risk of loss of resolution with each step.

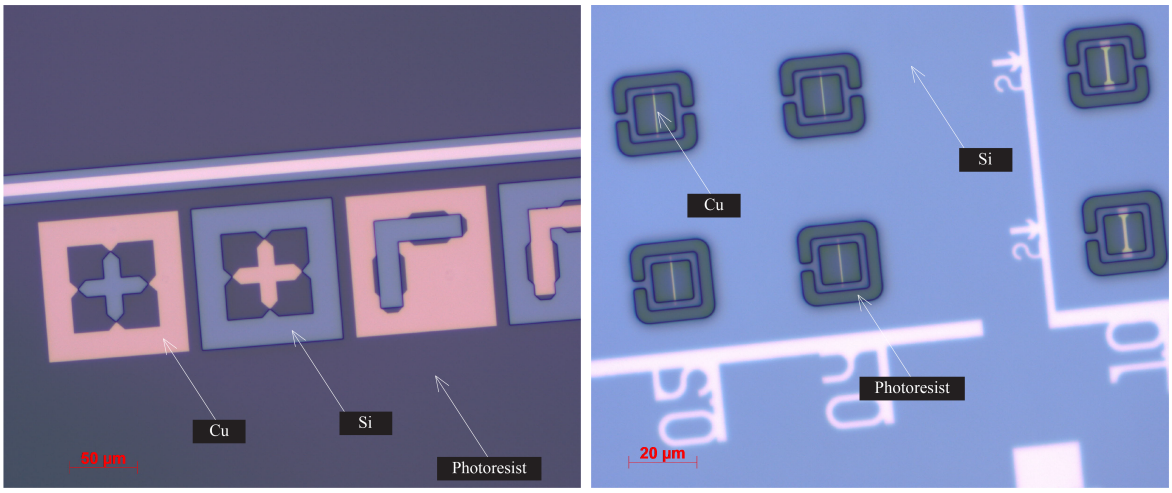

(a) (b)

Figure 3.10: Optical microscope image of (a) alignment marks from the sample deposition and patterned photoresist (b) patterned photo resist on top of copper test structures.

3.2.7 Step 7 - Aluminum frame deposition and lift off

The aluminum frame was deposited by e-beam evaporation as explained in section 3.2.3 using the VST machine. An aluminum thin film of 300 nm was deposited on the substrate to ensure the frame is rigid enough. The lift off was also carried out following the procedure outlined in section 3.2.4.

3.2.8 Step 8 - XeF_2 release

Xenon difluoride is known to isotropically etch silicon at ambient temperature with an etch rate that varies linearly with pressure [74]. In order to have a free standing test specimen, the SPTS Xactix e1 equipment was used to etch the silicon under the test

structure. The Xactix e1 equipment basically consists of chambers connected with pipes as show in figure 3.11. First the copper demonstrator is placed in the main chamber for a long pumped of 3 hours to ensure that chamber and sample is free of moisture [39]. Otherwise hydrogen fluoride is produced in the main chamber which poses the risk of an unwanted etching of the copper specimen.

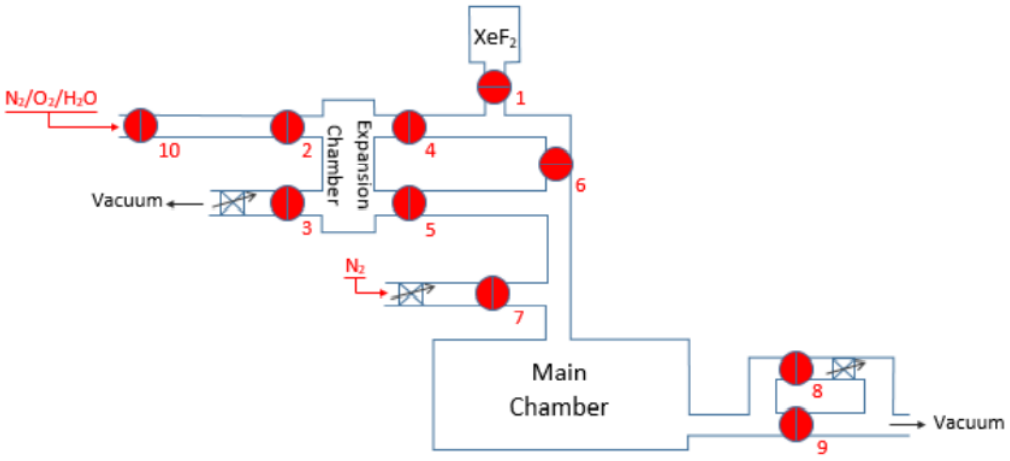

Figure 3.11: Schematic diagram showing the connections between the XeF_2 source, expansion chamber and main chamber of the Xactic e1 machine. [Source: Freely adapted from the control software].

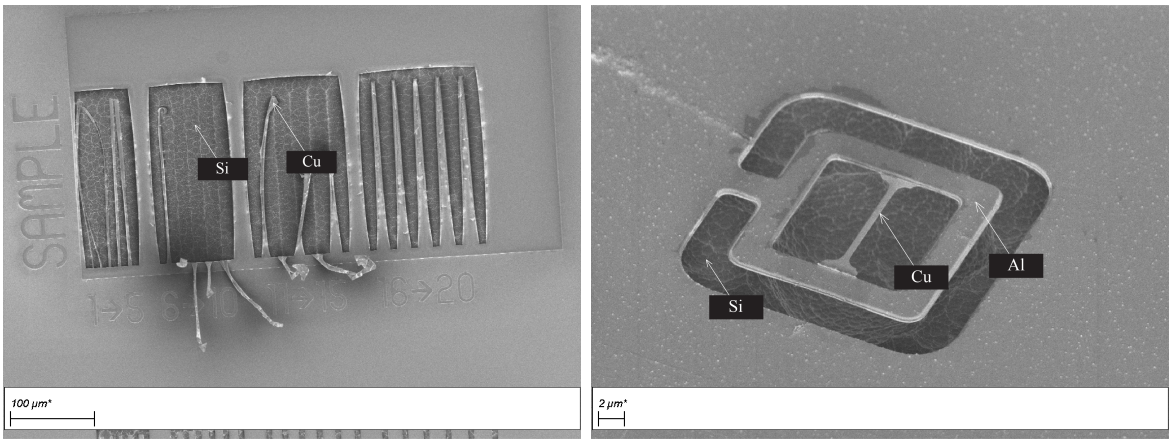

(a) (b)

Figure 3.12: SEM image of (a) fully released copper beams on a silicon substrate. The width of the copper beam increases from right to left. (b) fully released aluminum frame having a copper tensile test specimen in the middle ready for transfer unto the push-to-pull.

The next step was to vent the expansion chamber by injecting nitrogen gas to remove

any form of contaminant that may be present due to the previous use of the equipment. XeF_2 was then released into the expansion chamber until a pressure of 400 Pa is reached. The expansion chamber was then connected to the main chamber for a short pulse of 5-10 seconds for the actual etching of the silicon.The expansion chamber and the main chamber are thereafter purged with nitrogen gas. An image is taken before and after the etching on the monitor etch process. This entire step was repeated eight (8) times until the aluminum frame and the copper test specimen are fully released.

3.3 Graphene transfer

The concept of the aluminium frame for thin film manipulation was also extended to the manipulation of a graphene monolayer. In this case, the aluminum frame was fabricated using e-beam lithography instead of photolithography process described earlier. In fact the entire process was initially considered to be based on e-beam lithography mainly because of the high resolution obtainable $\sim 10nm$. The process was however time consuming and unfortunately, the e-beam lithography machine was not in the best possible service condition during the period of carrying out this work.

The aluminum frame process started with the standard cleaning (see section 3.2.1) of a standard silicon wafer cut into a square die using a diamond tip. Few droplets of a solution of 7% poly(methyl methacrylate) (PMMA) is then spincoated on the surface of the silicon wafer at a rotating speed of 4000 rpm for 60 seconds to have a resist thickness of 670nm as standardized in the WinFab. The wafer is then placed in the oven at 150 ^oC for 15 minutes to bake the PMMA. The pattern for the aluminum frame is then transferred unto the silicon substrate using the e-beam lithography machine which is a SEM that works in lithography mode. The final step is to develop the resin by first dipping the substrate in methyl isobutyl ketone (MIBK) for 1 minute 30 seconds and then dipped in an isopropyl alcohol (IPA) solution for 30 seconds. The substrate is then rinsed with IPA and dried with nitrogen gun. The substrate is then ready for aluminum metallization as described in section 3.2.3 using the VST machine. A lift off step is then done to remove the unwanted PMMA that still remains on the silicon substrate.

The structure is then released by etching silicon as described in section 3.2.8 to have a free standing aluminum frame. The graphene is then transferred unto the free standing aluminum frame following a process close to the one outlined by **Deokar *et al*** [75]

Figure 3.13: Schematic diagram showing (a) top view and (b) cross-sectional view of the silicon substrate after aluminum metallization and lift off.

and summarized in figure 3.14. A monolayer of graphene is first grown on a copper foil by chemical vapor deposition [76] which was then tapped unto a dummy silicon wafer along the edges of the graphene sheet. A solution of 7% PMMA was then spin coated on the graphene sheet at 6000 rpm for 60 seconds in order to prevent the graphene from damage during the transfer. The PMMA is then allowed to dry for 24 hours at room temperature. The next step is therefor the etch the copper foil under the graphene sheet. This was done by carefully detaching the PMMA/graphene/copper structure from the silicon wafer and gently placed on a 0.5M solution of ammonium persulfate ($(NH_4)_2S_2O_8$) for 15 hours. With the copper foil etched away, the PMMA/graphene stack was rinsed by floating it on DI water for 8 hours to remove contaminants from the copper foil and the etchant solution.

A blotting paper is then used to extract the PMMA/graphene stack from the DI solution and then transferred unto the aluminum frame structure after waiting for 10 minutes for natural removal of water underneath the graphene. Fresh PMMA was then spincoated on the PMMA/Graphene stack to dissolve the previous PMMA before placing the whole structure in acetone for 20 minutes at 60^oC to remove the PMMA. The graphene is then gently rinsed with acetone, methanol and water in succession and then dried nitrogen gun.

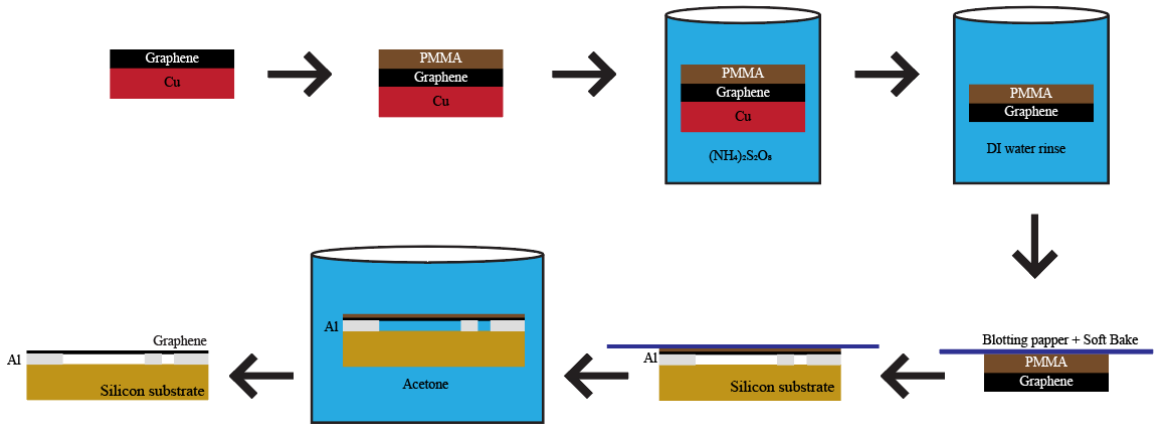

Figure 3.14: Schematic diagram showing (a) top view and (b) cross-sectional view of the silicon substrate after aluminum metallization and lift off.

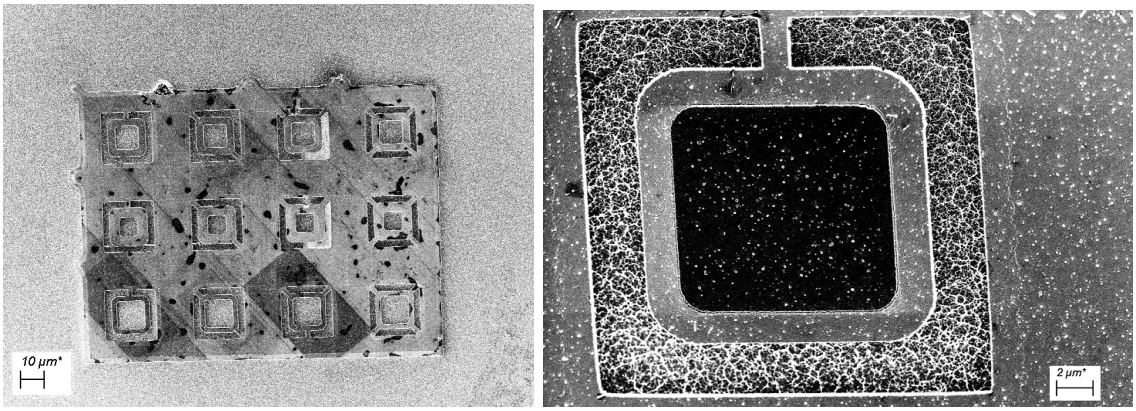

(a) (b)

Figure 3.15: SEM image of (a) graphene monolayer transferred unto an array of free-standing aluminum frames (b) close-up view of one of the aluminum frame with a graphene monolayer on top of the frame.

3.4 Transfer of frame-sample structure onto the PTP

The push-to-pull developed by Hystron Incorporated [19] was used for in-situ tensile testing in TEM in this current work (see figure 3.16). A picoindenter that can work either in load- or displacement- controlled mode was used alongside the PTP. The load control mode was used due to the unreliability of the displacement controlled mode.

The transfer of the frame-sample structure onto the PTP for uniaxial testing was carried out at the Electron Microscopy for Material Science (EMAT) facility of University of

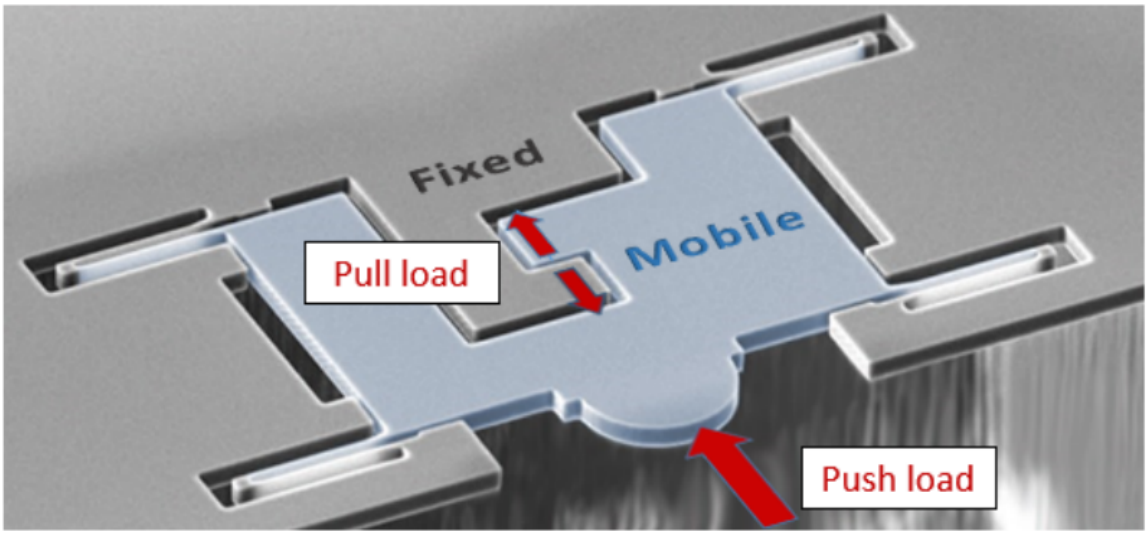

Figure 3.16: SEM image of Push-to-Pull device showing the mobile and fixed part.

Antwerp. The transfer and manipulation of the frame-sample structure was performed in the SEM-FIB machine that is equipped with a nano-manipulator(tungsten tip). The process essentially involves the detaching of the frame by cutting the anchor with FIB then welding onto the push to pull.

3.4.1 Detaching the frame from the grid

This step involves the detachment of one of the frames from the grid by cutting the anchor with FIB. First the nano-manipulator has to be fixed onto one of the edges of the frame before the FIB cutting of the anchors otherwise the frame would fall off and the sample can be damaged. Thus the tungsten tip is carefully brought in contact with the aluminum frame guided by the live image recorded with the SEM. The tip is then welded to the frame by ion beam induced deposition of platinum around the tip to ensure it is firmly gripping the frame. It is important to note that this step could serve as a source of platinum contaminant for the sample, hence the welded as far as possible from the sample area preferable close to the edge of the frame. In this present work, the tungsten tip was attached to the frame with only one anchor having a copper tensile specimen in the middle. This allows for flexibility with the attachment of the tungsten tip.

Secondly, the anchor point holding the frame to the grid is then cut using FIB of Ga^+ ions. As mentioned in section 3.1, the use of Ga^+ for cutting posses a significant

challenge. Even though this was not directly used for cutting the sample in this present work, the chances of gallium re-deposition on the sample cannot be fully ruled out. The more reason why the lateral dimensions of the frame was made as wide as possible. Meanwhile when compared to the previous work by Gillet, the number of anchors have been greatly reduced from eight (8) anchor points [1] to only one anchor point. This does not only reduce the chances of Ga^{+} re-deposition, it also saves time required to cut the eight (8) anchor points by FIB milling. Once this step is completed, the frame is then fully detached from the grid and is ready to be transferred onto the PTP. Figure 3.17 shows the procedure for the detachment of the frame from the grid.

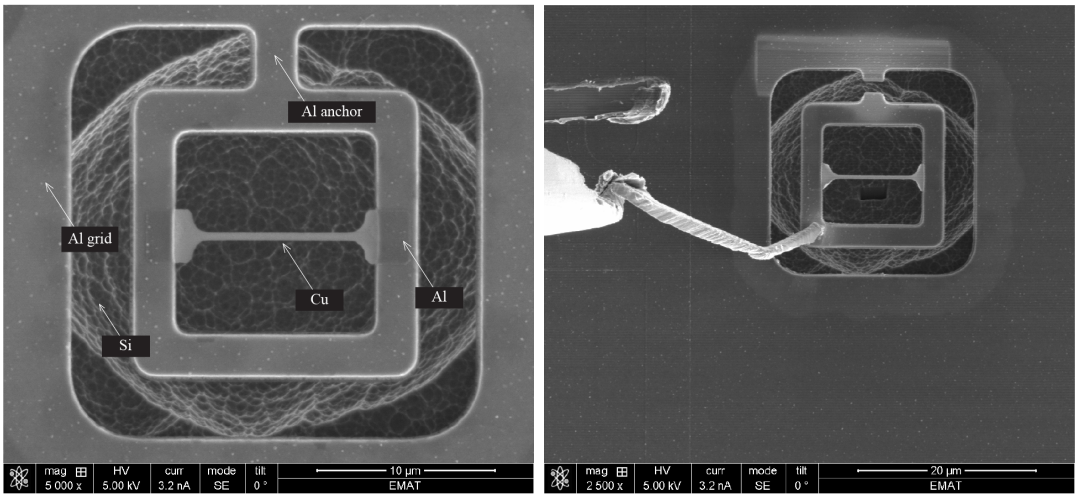

(a) (b)

Figure 3.17: SEM image of Free standing aluminum frame having a tensile copper specimen in the middle (a) before detaching from the grid (b) after detaching from the grid.

3.4.2 Fixing the frame onto the PTP by EBID

Here the detached frame-sample structure is transferred onto the PTP then re-attached using electron beam induced deposition of platinum on the edges of the frame. The nano-manipulator was used to slightly push the frame on the PTP to make the welding of one of the edges of the frame before detaching the tungsten tip from the frame by FIB cutting. The other edges of the frame were then welded onto the PTP after the detachment of the tungsten tip. The final step before the traction test is to cut the sides of the frame that lies parallel to the tensile sample. This way, when the tensile test is performed with the PTP, the force can be transferred unto the sample. Figure

3.18 shows a successfully transferred frames-sample structure ready for *in-situ* tensile testing in the TEM.

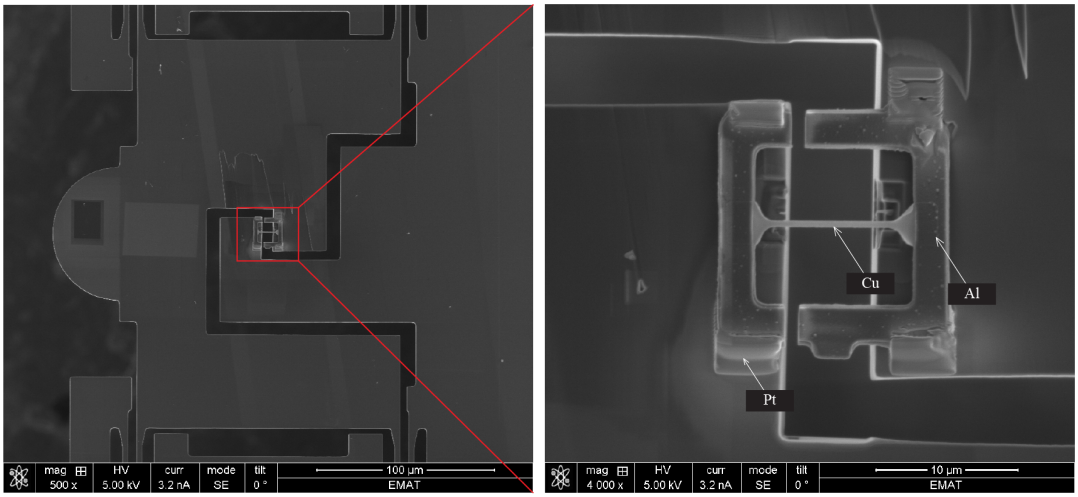

(a) (b)

Figure 3.18: SEM image of (a) frame-sample structure successfully transferred onto and attached to the PTP by EBID, (b) zoomed in view of the gap area of the PTP where the frame-sample structure is placed.

3.5 In-situ tensile testing in TEM

A Hysitron PI-95 PicoIndenter [65] and the PTP device were used for the tensile test of the copper thin film. The experiment was carried out in the column of the FEI-Osiris microscope at EMAT operating at 200 kV. The PicoIndenter is essentially a transducer that applies normal force only consisting of a force/displacement sensor; drive circuit board and a means to mount the transducer onto the TEM. The design of the PTP is such that the compressive force applied to the movable part is converted into tensile load thanks to the folded springs connecting the movable to the fixed part of the PTP. The nominal stiffness of the PTP used for the experiment was $450N/m$ at a loading rate $0.1\mu N/sec$ under load-controlled. The magnitude of the applied force on the specimen was determined by subtracting the contribution of the spring stiffness from the raw force while the displacement was determined by digital image correlation method [21, 77]. The experiment was performed until the fracture of the copper thin film.

As seen in figure 3.19, the copper thin film appeared to have failed by brittle fracture after about 75 seconds into the test. A zoomed in view of the fracture area after

(a) t = 0 sec (b) t = 20 sec (c) t = 40 sec (d) t = 60 sec (e) t = 75 sec

Figure 3.19: Snapshots of the change in length of the copper thin film during the tensile testing.

the tensile test is shown in figure 3.20b. Indeed more information about the in-situ deformation of the copper thin film would be easily accessed with a tensile specimen having a gauge length of at most 2 µm. This way it will be possible to perform the test at higher magnification.

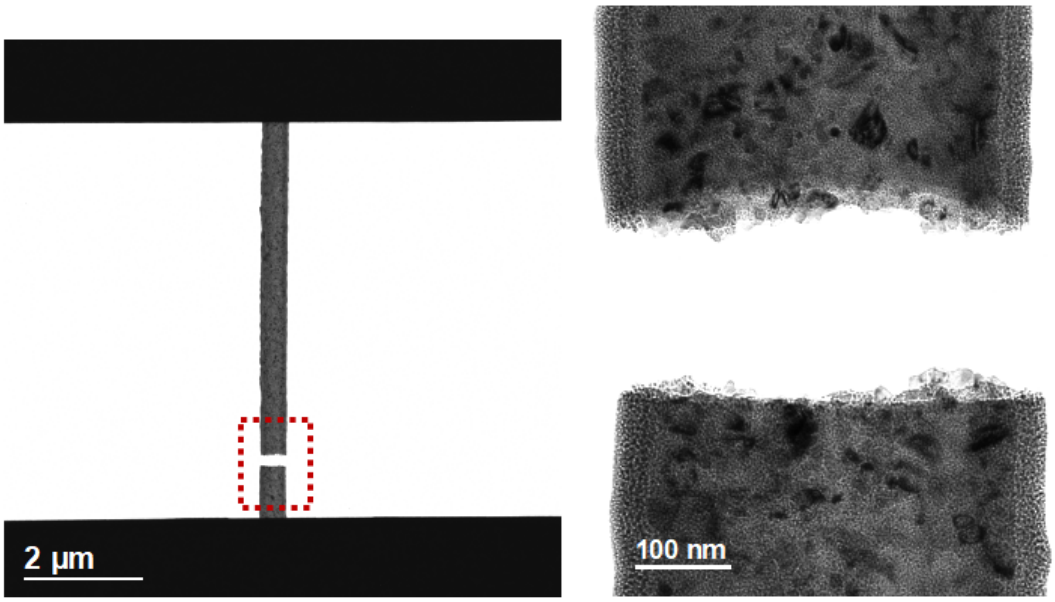

(a) (b)

Figure 3.20: In-situ TEM images of the copper thin film (a) after the tensile test (b) zoomed in area of the fracture area after the tensile test.

Chapter 4

Results and Discussion

This thesis work reports some interesting results listed below:

- the successful manipulation and transfer of an ultra thin copper film ($\sim 30nm$) onto a Push-to-Pull device for in-situ tensile testing in the TEM. This was previously impossible owing to the presence of internal stress in thin film structure;
- the use of optical lithography to achieve the printing of sub-micron ($< 1\mu m$) features onto a substrate owing to the adapted lithography parameters in this present work;
- this present work also present a more straight forward approach in terms of the frame-sample fabrication process when compared to the previous work of **Gillet** [1].

The above mentioned results as well as the challenges faced during this thesis work will be discussed in this present section. Possible solutions and further perspectives on optimization of the process steps will also be considered as a basis of discussion.

4.1 Internal stress consideration

As mentioned in section 3.2.3, a separate silicon wafer was prepared to determine the internal stress present in each of the copper, aluminum and alumina thin film used as demonstrators. This was done by applying the Stoney formula in equation 3.1. The radius of curvature of the wafer before and after the thin film deposition are are

presented in table 4.1.

Material	$R_0(\mu m)$	R after deposition (µm)	R after three (3) days (µm)
Al (sample)	418.36 $\times 10^6$	334.72 $\times 10^6$	268.86 $\times 10^6$
Al_2O_3	197.26 $\times 10^6$	190.95 $\times 10^6$	183.43 $\times 10^6$
Cu	465.76 $\times 10^6$	540.60 $\times 10^6$	413.80 $\times 10^6$
Al (frame)	138.98 $\times 10^6$	109.87 $\times 10^6$	109.48 $\times 10^6$

Table 4.1: Measured radius of curvature before, immediately after and three days after the thin film deposition.

The remaining parameters required for determining the internal stress in thin film based on the Stoney formula are the Young modulus and Piosson ratio of the silicon substrate which is given as 140 GPa and 0.265 respectively. The thickness of the deposited thin film and the silicon substrate were also measured and presented in table 4.2

Material	$t_f(nm)$	$t_s(\mu m)$
Al (sample)	31	390
Al_2O_3	32	395
Cu	30	393
Al (frame)	325	390

Table 4.2: Measured thickness of the deposited thin film (t_s) and substrate (t_f) onto which it was deposited.

The parameters in table 4.1 and 4.2 allows for the computing of the internal stress present in the thin film by applying equation 3.1. This results is presented in table 4.3.

Material	σ_f after deposition (MPa)	σ_f three (3) days after deposition (MPa)
Al (sample)	-930.3	-206.9
Al_2O_3	-24.0	-54.7
Cu	43.7	-40
Al (frame)	-30.7	-31.2

Table 4.3: Measured thickness of the deposited thin film (t_s) and substrate (t_f) onto which it was deposited.

Indeed the internal stress in the copper sample was revealed after the XeF_2 release step as show in figure 3.12a. It would be practically impossible to manipulate the copper beam in this already deformed condition which was the main reason for applying the

concept of the aluminum frame. The difference with the use of the aluminum frame to hold the copper thin film in place indeed made the manipulation possible without deformation of the copper thin film as shown in figure 3.12b. Thus the feasibility of the manipulation of very thin and fragile samples have been validated by this thesis work.

4.2 Frame-sample fabrication process optimization

As mentioned in the introductory section of this thesis work, an objective of this thesis work is to implement an optimized fabrication process for the frame-sample structure. This is done in comparison with the previous work by **Gillet** [1]. The major considerations include the material selection for the frame, the frame design parameter and the reproducibility of the fabrication process.

4.2.1 Frame material selection

The key parameters considered for the selection of the frame material are the material stiffness and the internal stress state of the thin film after the release step. It is required that the frame material sufficiently stiff and should have a minimal internal stress. Otherwise the expression of the internal stress present in the frame material after the release step will deform the material even before the in-situ tensile test. Lastly the selected material should be amenable to the different clean room reagents without compromising its integrity. It is also important to note that the material selected for the frame would naturally inform the fabrication process route.

In the previous work [1], silicon was proposed as the material for the frame while aluminum was used in this present work. The specific strength versus specific modulus of different material is shown on the Ashby map in figure 4.1. The chart shows a comparative advantage of silicon over aluminium. Moreso silicon is a common material used in the clean room for the fabrication of MEMS device. Aluminum is however selected as the frame material in this present work because it possesses the strict requirement of non-reactivity with XeF_2 [79] while silicon is know to be selectively etched by XeF_2 . It is also know to contain moderate levels of internal stress when deposited by evaporation which is a critical requirement of the frame.

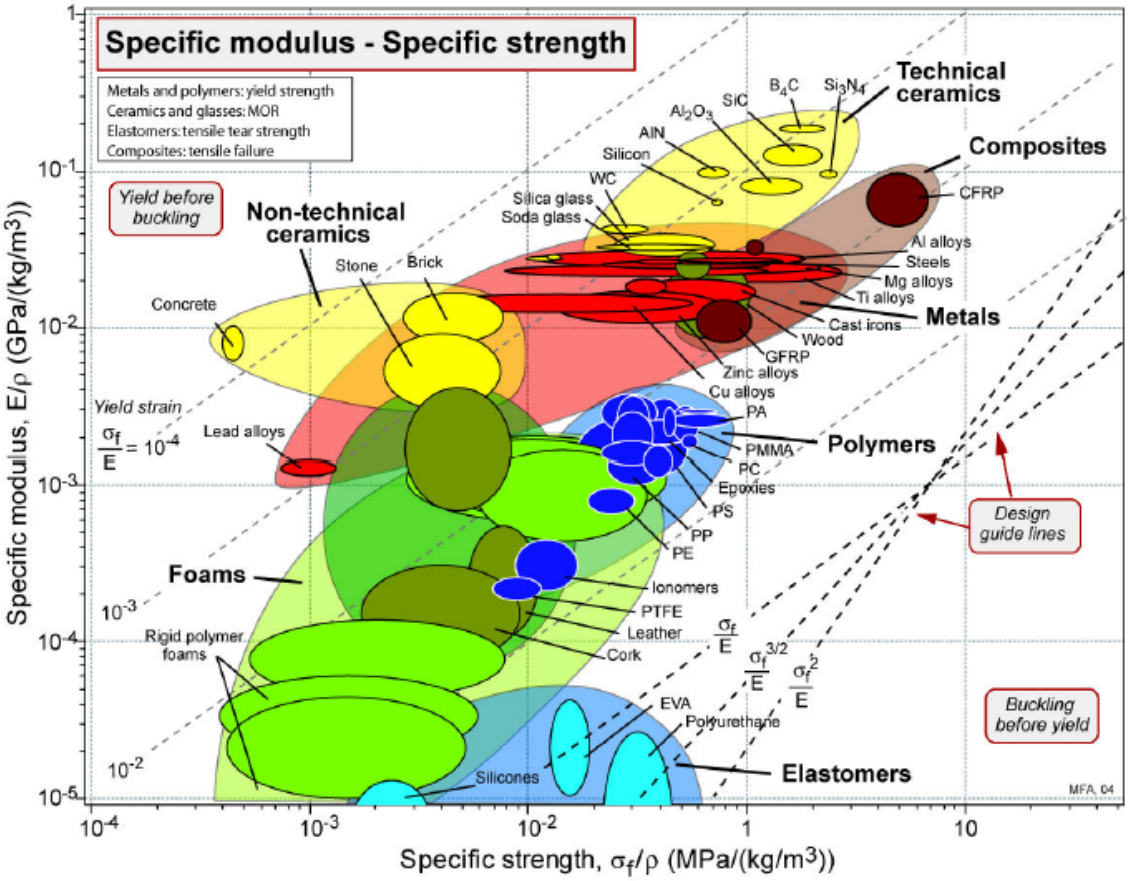

Figure 4.1: Material selection chart showing the specific strength versus the specific modulus of different material classes. [78]

4.2.2 Frame design parameter

The frame design for this present work (design A) draws inspiration from the previous work [1] and the conceptual designs from both works are placed side by side in figure 4.2. The lateral dimensions of design A have largely been unchanged when compared to design B. The number of anchors have largely been reduced from eight (8) to only one (1) between design A and B. This was implemented bearing in mind that at some point during the transfer of the frame onto the push-to-pull device, the anchors needs to be cut by FIB as described in section 3.4.1.

Of course, it can be envisaged that reducing the number of anchors could have a negative impact on the mechanical stability of the frame however,it would be a gain in time as there will be less FIB cutting and also pose less risk to the sample contamination.

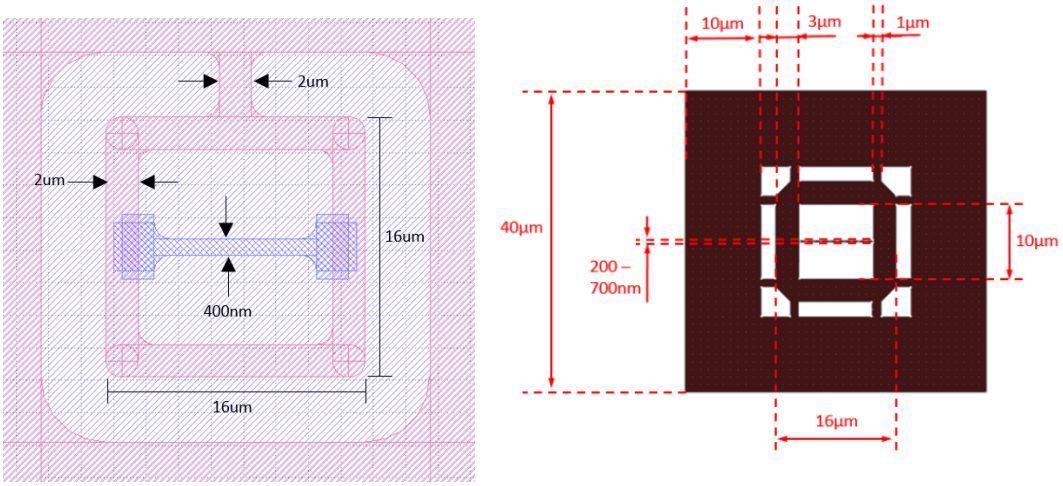

(a) (b)

Figure 4.2: Conceptual designs from (a) this current work and (b) the previous work [1].

This was indeed successfully implemented with a careful look at figure 3.12b. There was no observable negative impact on the mechanical stability of the frame which could be attributed to the fact that the thickness of the frame (around 300nm) was sufficient.

In addition, design A attempted at implementing a "dog-bone" shaped tensile sample instead of a beam for the sample part of the structure as shown in design B. The idea is to mirror what would be obtainable during a macroscopic tensile testing procedure. As such the gauge length of the "dog-bone" structure was set as set at 8 µm to ensure that the sample runs over the gap of the push-to-pull ($\sim 2.5\mu m$) during the tensile test. Lastly, design A ensured that sharp edges are avoided as much as possible to mitigate the risk of stress concentration at the edges which could lead to premature failure of the structure. In summary, the changes made on design B were successfully implemented with little or no negative effect to the stability of the frame.

4.2.3 Fabrication process flow

Another point of discussion is to consider the fabrication process employed in this present work (Process A) with respect to the process employed in the previous work by **Gillet** [1] (Process B). Both processes are shown in figure 4.3. Process A appears to have an extra process step however the entire fabrication process is based optical

lithography repeated twice. The critical step in this process is indeed the alignment step during the second photolithography at step at step 6.

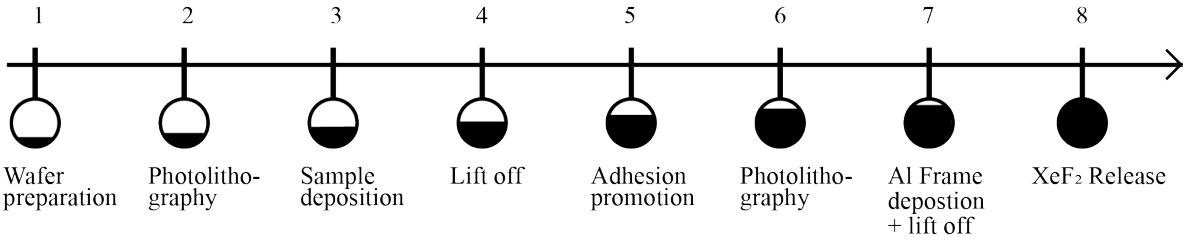

(a) Process A

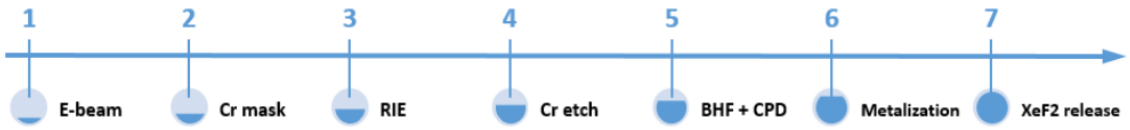

(b) Process B [1]

Figure 4.3: General overview of frame-sample fabrication process.

Process B has two critical process steps which are the reactive ion etching and buried oxide layer etching at step 3 and step 6 respectively.

4.3 EDX result of copper sample

Another main objective of this thesis work is to ensure that the sample part of the frame-sample structure is free from contamination. This is to ensure that the mechanical properties obtained from the in-situ tensile test is representative of the sample and not influence by impurities. The major sources of impurities comes gallium due to FIB milling and platinum from the welding by IBID. This is the reason why photolithography have been used for the frame-sample fabrication such that the sample is not cut by FIB throughout the entire fabrication process and the nano-welding is done on the frame and not on the sample (see figure 3.17b and 3.18b). The results from the Energy-dispersive X-ray spectroscopy (EDX) analysis performed along the edge and across the width of the copper specimen are shown in figure 4.4 and figure 4.6 respectively.

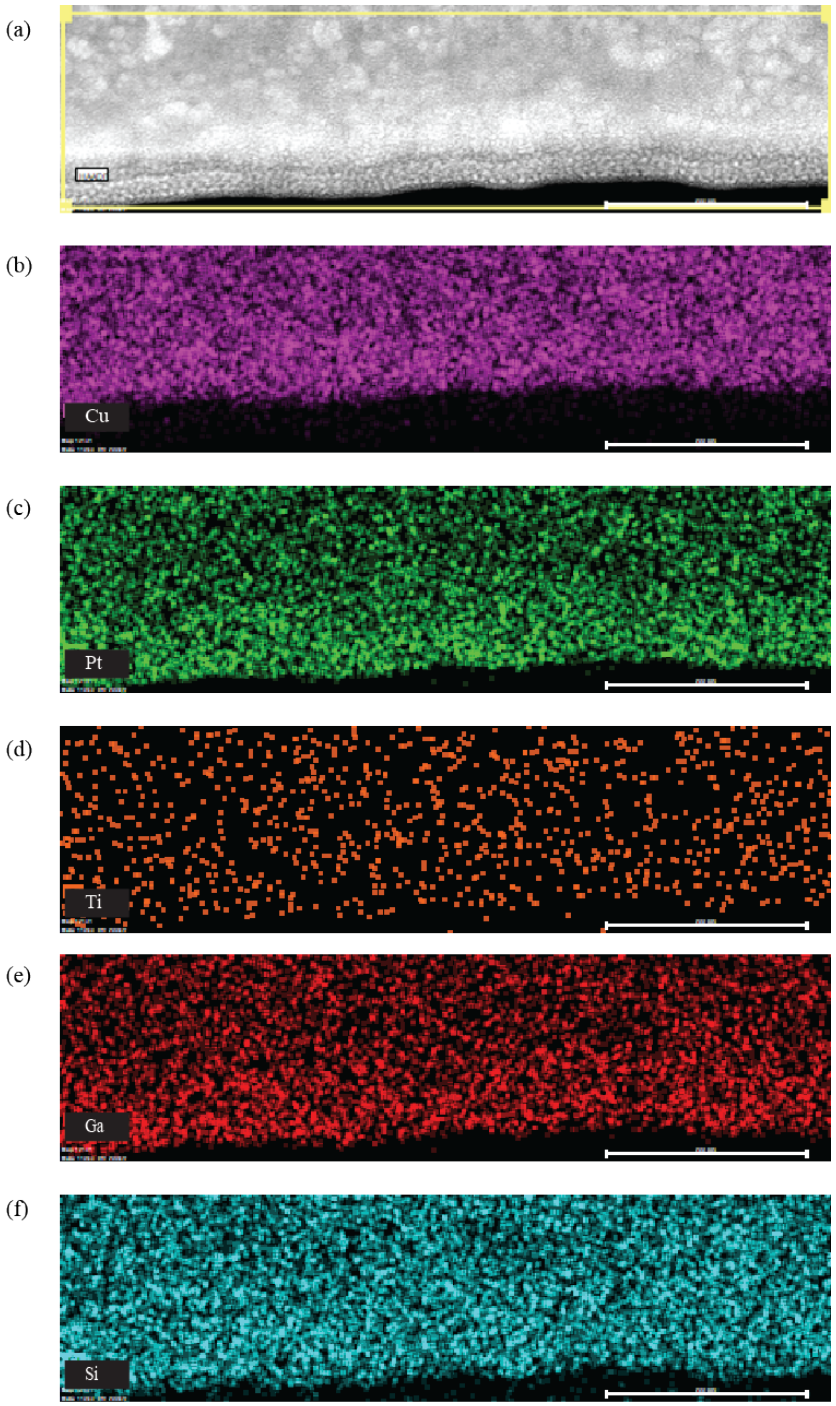

Figure 4.4: Result from the EDX experiment performed on the sides of the copper sample.

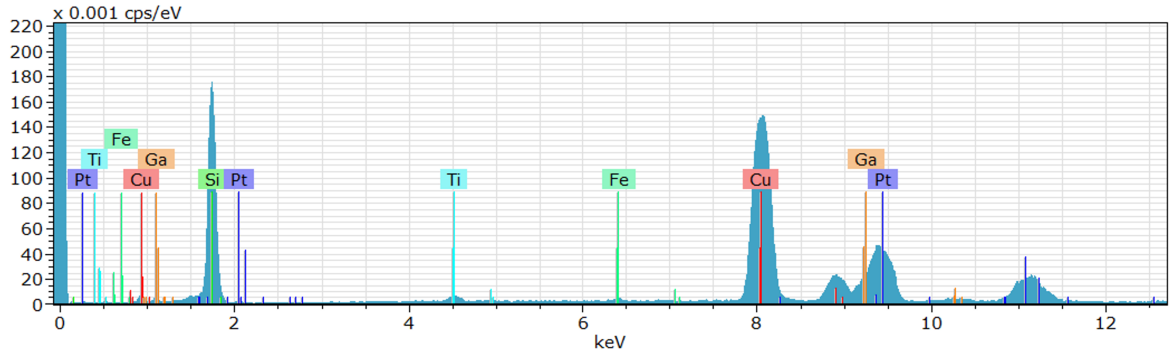

Figure 4.5: EDX spectrum showing the peaks of the individual elements observed during the EDX analysis performed along the edge of the copper sample.

Element	Series	wt%	at %
Copper	K-series	30.28	46.86
Platinum	L-series	58.18	29.32
Silicon	K-series	3.54	12.42
Gallium	K-series	7.79	10.98
Titanium	K-series	0.19	0.39
	Sum	100	100

Table 4.4: Quantification of the amount of elements in wt% and at% for the EDX analysis performed along the edge of the copper sample.

The results from the EDX analysis reveals that the sample is not free from contamination. Elements such as gallium, platinum, silicon, titanium and aluminum are present both along the edges and across the with of the copper sample (see figure 4.4 and figure 4.6). The amount of the impurity elements were quantified and presented in table 4.4 and table 4.5. These results reveal an unusually high amount of platinum contamination the source of which could be due to the nano-welding of the frame onto the PTP.

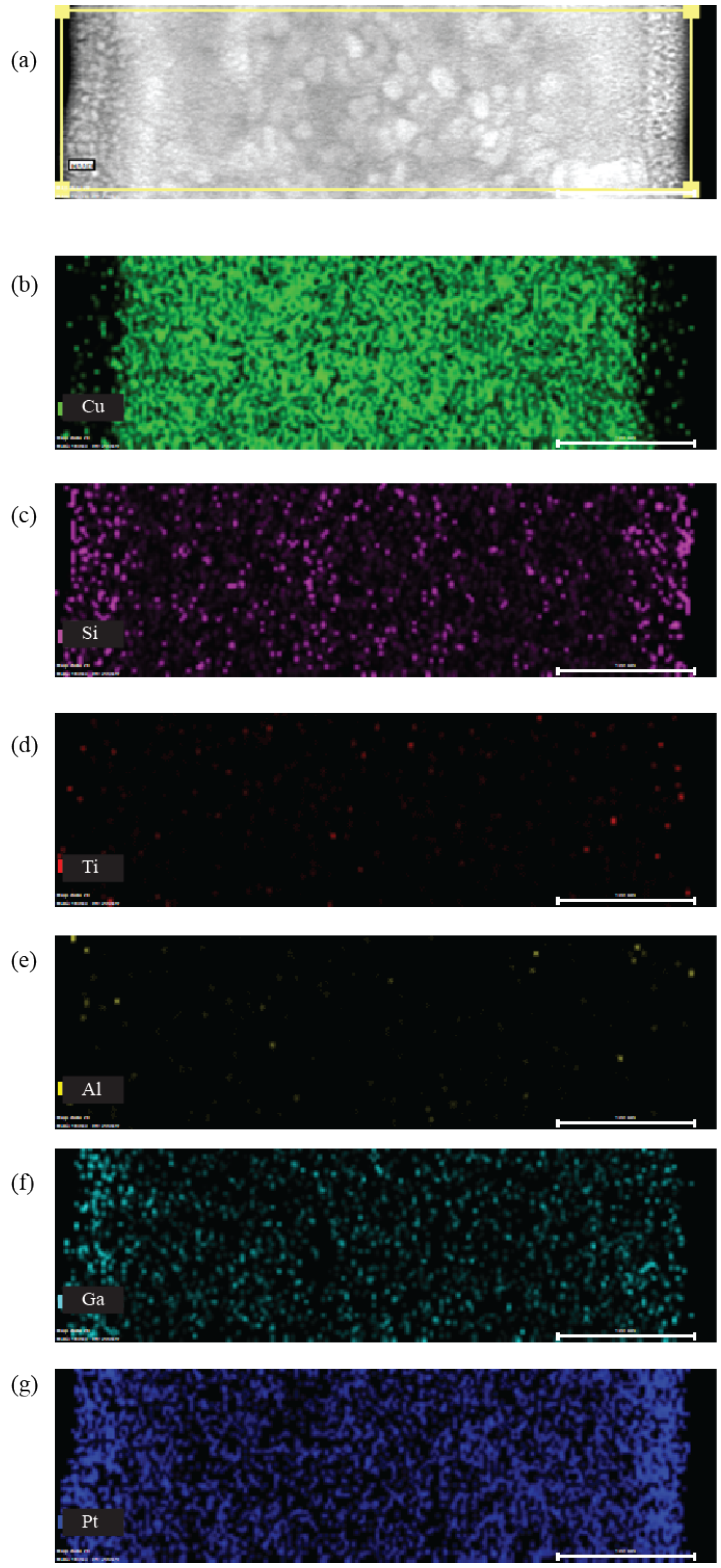

Figure 4.6: Result from the EDX experiment performed on across the width of the copper sample.

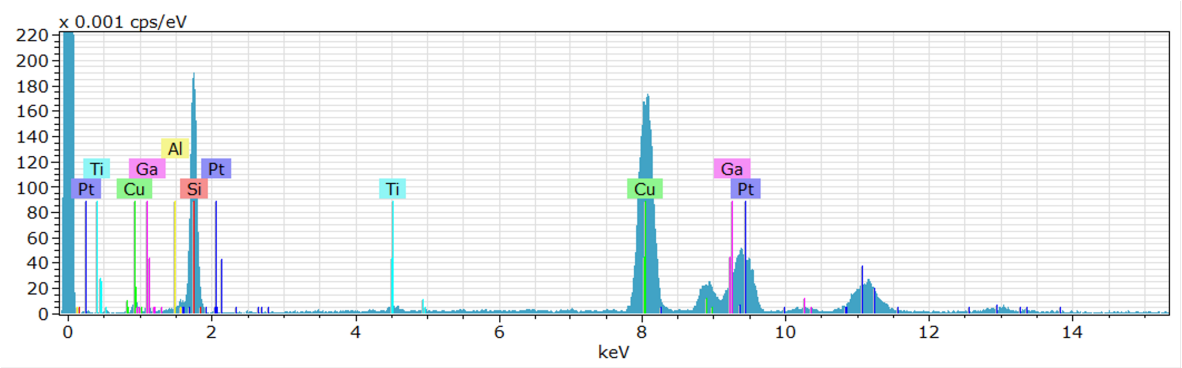

Figure 4.7: EDX spectrum showing the peaks of the individual elements observed during the EDX analysis performed across the width of the copper sample.

Element	Series	wt%	at %
Copper	K-series	30.16	46.92
Platinum	L-series	58.77	29.78
Silicon	K-series	3.49	12.31
Gallium	K-series	7.24	10.26
Titanium	K-series	0.28	0.59
Aluminium	K-series	0.036	0.13
	Sum	100	100

Table 4.5: Quantification of the amount of elements in wt% and at% for the EDX analysis performed across the width of the copper sample.

4.4 Tensile properties determination

In order to compute the stres-strain curve of the copper sample, the following assumptions were made;

- The set up of the frame-sample structure attached to the PTP is rigid, meaning that the displacement in the gap of the PTP is equal to the displacement on the sample.
- There is perfect contact between the frame and the sample.
- The contribution of the deformation of the frame to the total deformation of the sample is ignored.

Thus the corrected load on the sample is given by equation 4.1.

$$F_s = F_t - (K_p \triangle l) \tag{4.1}$$

Where F_s = corrected load on the sample
F_t = total load recorded on the picoindenter.
K_p = stiffness of the PTP
$\triangle l$ = displacement of the gap of the PTP.

The stress on the sample is then computed by normalizing the corrected force on the sample by the cross sectional area of the sample (equation 4.2) while the strain is calculated by PTP gap displacement by the gauge length of the sample (equation 4.3). The resulting stress-strain curve is shown in figure 4.8.

$$\sigma_s = \frac{F_s}{A_s} \tag{4.2}$$

$$\epsilon_s = \frac{\triangle l}{l_0} \tag{4.3}$$

A total strain of 0.107 [-] and a maximum stress of 3.5 GPa can be observed from the plot. This result may need to be validated owing to the assumptions that have been made.

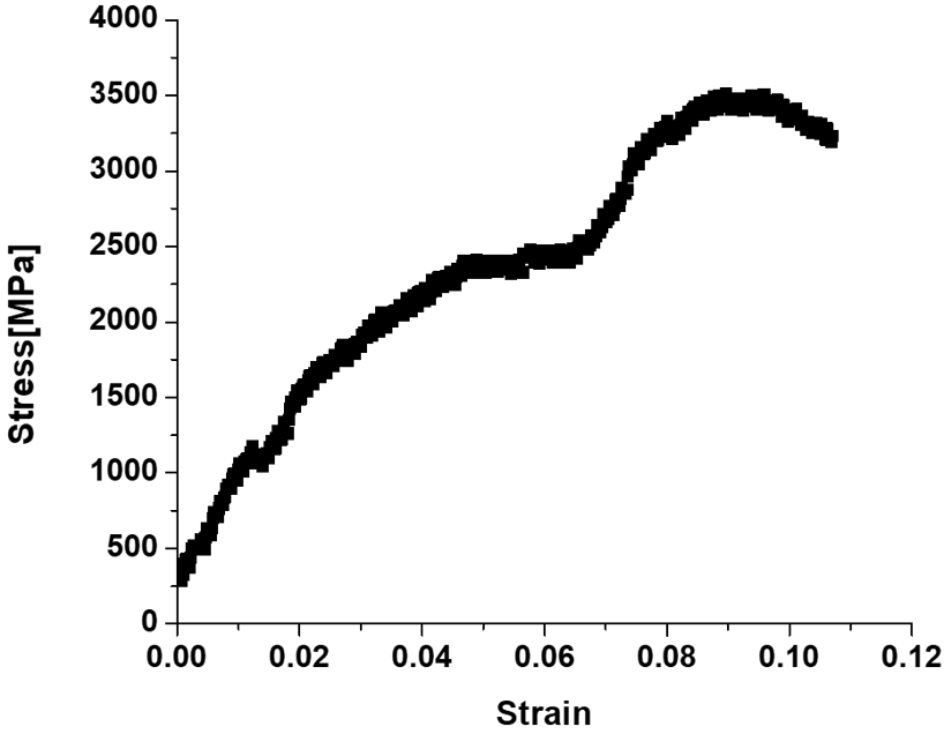

Figure 4.8: Stress-strain curve

Chapter 5

Conclusion and Further Perspectives

This master thesis aimed at the fabrication of new aluminum frame for in-situ tensile testing in TEM. The two objective of this work were; *(i)* to totally avoid the use of FIB milling for the sample preparation, *(ii)* to perform a successful manipulation and transfer of an ultra thin ($<$ 50nm) tensile specimen onto a push-to-pull device and *(iii)* to ensure that the prepared tensile sample is free from contamination. The feasibility of the first two objectives have been demonstrated for a 30nn copper thin film. Three other materials namely alumina, aluminium and graphene were also planned as demonstrators. The fabrication process for the aluminum and alumina demonstrators stopped at step 4 and step 6 respectively. Nevertheless some improvements can be proposed. E-beam evaporation can be considered for the deposition of the aluminum thin film instead of sputtering because the latter provides a non-comformal deposition which is best suited for lift-off. A metallic layer can also be deposited before in order to enhance the alignment step in the case of alumina demonstrator. Due to time constraint, the characterization of the graphene sample was not carried out so it is still unclear if the graphene transfer process was successful and if the concept of the frame can be applied to a monolayer of graphene.

Another important conclusion that can be drawn from this work is that optical lithography can be used to obtain sub-micronic features on a silicon substrate. Finally, concerning the in-situ tensile test carried out on the copper sample, a number of approximations have been made and the results may need to be validated. It is also suggested to reduce

the gauge of the tensile sample to a maximum of 2µm in other to have a clearer view of the deformation area during the in-situ tensile testing. This way, more information about the underlying deformation mechanism for ultra thin films can be extracted.

Bibliography

[1] Julien GILLET. "Mechanical Testing of Nano-materials XeF_2-based design of freestanding nanometre-sized thin film samples for in-situ TEM tensile testing." Master thesis, Université catholique de Louvain, 2016.

[2] Zhong Lin Wang and Jinhui Song. "Piezoelectric nanogenerators based on zinc oxide nanowire arrays". In: *Science* 312.5771 (2006), pp. 242–246.

[3] Candace K Chan et al. "High-performance lithium battery anodes using silicon nanowires". In: *Nature nanotechnology* 3.1 (2008), pp. 31–35.

[4] Xiao Hua Liu et al. "In situ atomic-scale imaging of electrochemical lithiation in silicon". In: *Nature nanotechnology* 7.11 (2012), pp. 749–756.

[5] XL Feng et al. "Very high frequency silicon nanowire electromechanical resonators". In: *Nano Letters* 7.7 (2007), pp. 1953–1959.

[6] Owen Y Loh and Horacio D Espinosa. "Nanoelectromechanical contact switches". In: *Nature nanotechnology* 7.5 (2012), p. 283.

[7] Michael C McAlpine et al. "High-performance nanowire electronics and photonics on glass and plastic substrates". In: *Nano letters* 3.11 (2003), pp. 1531–1535.

[8] Zhiyong Fan et al. "Toward the development of printable nanowire electronics and sensors". In: *Advanced Materials* 21.37 (2009), pp. 3730–3743.

[9] Seung Yoon Ryu et al. "Lateral buckling mechanics in silicon nanowires on elastomeric substrates". In: *Nano letters* 9.9 (2009), pp. 3214–3219.

[10] Feng Xu, Wei Lu, and Yong Zhu. "Controlled 3D buckling of silicon nanowires for stretchable electronics". In: *Acs Nano* 5.1 (2011), pp. 672–678.

[11] Shanshan Yao and Yong Zhu. "Nanomaterial-enabled stretchable conductors: strategies, materials and devices". In: *Advanced materials* 27.9 (2015), pp. 1480–1511.

[12] Yong Zhu and Tzu-Hsuan Chang. "A review of microelectromechanical systems for nanoscale mechanical characterization". In: *Journal of Micromechanics and Microengineering* 25.9 (2015), p. 093001.

[13] Shaoning Lu et al. “Realization of nanoscale resolution with a micromachined thermally actuated testing stage”. In: *Review of Scientific Instruments* 75.6 (2004), pp. 2154–2162.

[14] Shaoning Lu et al. “In situ mechanical testing of templated carbon nanotubes”. In: *Review of scientific instruments* 77.12 (2006), p. 125101.

[15] Mario Kiuchi, Shinji Matsui, and Yoshitada Isono. “Mechanical characteristics of FIB deposited carbon nanowires using an electrostatic actuated nano tensile testing device”. In: *Journal of microelectromechanical systems* 16.2 (2007), pp. 191–201.

[16] Joseph J Brown et al. “Microsystem for nanofiber electromechanical measurements”. In: *Sensors and Actuators A: Physical* 155.1 (2009), pp. 1–7.

[17] PolyMUMPS Service. “MEMSCAP, Inc”. In: *Research Triangle Park, NC,USA* ().

[18] JJ Brown et al. “Tensile measurement of single crystal gallium nitride nanowires on MEMS test stages”. In: *Sensors and Actuators A: Physical* 166.2 (2011), pp. 177–186.

[19] Shan Z W Oh Y Cyrankowski E and Asif S A S. “Micro/nano-mechanical test system employing tensile test holder with push-to-pull transformer US Patent: US20100095780 Al”. In: (2010).

[20] Hua Guo et al. “Mechanics and dynamics of the strain-induced M1–M2 structural phase transition in individual VO2 nanowires”. In: *Nano letters* 11.8 (2011), pp. 3207–3213.

[21] Hosni Idrissi et al. “Low-temperature plasticity of olivine revisited with in situ TEM nanomechanical testing”. In: *Science advances* 2.3 (2016), e1501671.

[22] Y Lu, Y Ganesan, and J Lou. “A multi-step method for in situ mechanical characterization of 1-D nanostructures using a novel micromechanical device”. In: *Experimental mechanics* 50.1 (2010), pp. 47–54.

[23] Yang Lu et al. “Quantitative in situ TEM tensile testing of an individual nickel nanowire”. In: *Nanotechnology* 22.35 (2011), p. 355702.

[24] Mohammad Naraghi et al. “Novel method for mechanical characterization of polymeric nanofibers”. In: *Review of scientific instruments* 78.8 (2007), p. 085108.

[25] L Reimer and A Schmidt. “The shrinkage of bulk polymers by radiation damage in an SEM”. In: *Scanning* 7.1 (1985), pp. 47–53.

[26] Md Amanul Haque and M Taher A Saif. “In-situ tensile testing of nano-scale specimens in SEM and TEM”. In: *Experimental mechanics* 42.1 (2002), pp. 123–128.

[27] Yong Zhu, N Moldovan, and Horacio D Espinosa. "A microelectromechanical load sensor for in situ electron and x-ray microscopy tensile testing of nanostructures". In: *Applied physics letters* 86.1 (2005), p. 013506.

[28] Yong Zhu and Horacio D Espinosa. "An electromechanical material testing system for in situ electron microscopy and applications". In: *Proceedings of the National Academy of Sciences* 102.41 (2005), pp. 14503–14508.

[29] Guangming Cheng et al. "Mechanical properties of silicon carbide nanowires: effect of size-dependent defect density". In: *Nano letters* 14.2 (2014), pp. 754–758.

[30] Qingquan Qin et al. "Recoverable plasticity in penta-twinned metallic nanowires governed by dislocation nucleation and retraction". In: *Nature communications* 6.1 (2015), pp. 1–8.

[31] MS Steighner et al. "Dependence on diameter and growth direction of apparent strain to failure of Si nanowires". In: *Journal of Applied Physics* 109.3 (2011), p. 033503.

[32] Dongfeng Zhang et al. "In situ tensile testing of individual Co nanowires inside a scanning electron microscope". In: *Nanotechnology* 20.36 (2009), p. 365706.

[33] Lisa Y Chen et al. "Lattice anharmonicity in defect-free Pd nanowhiskers". In: *Physical review letters* 109.12 (2012), p. 125503.

[34] Marie-Stéphane Colla. "Plasticity and creep in thin free-standing nanocrystalline Pd films". PhD thesis. PhD thesis, Université catholique de Louvain, 2014.

[35] Hosni Idrissi et al. "Ultrahigh strain hardening in thin palladium films with nanoscale twins". In: *Advanced Materials* 23.18 (2011), pp. 2119–2122.

[36] Bailiang Wang et al. "Advanced TEM investigation of the plasticity mechanisms in nanocrystalline freestanding palladium films with nanoscale twins". In: *International journal of plasticity* 37 (2012), pp. 140–156.

[37] M-S Colla et al. "High strength-ductility of thin nanocrystalline palladium films with nanoscale twins: on-chip testing and grain aggregate model". In: *Acta Materialia* 60.4 (2012), pp. 1795–1806.

[38] Michaël Coulombier. "Nanomechanical lab on-chip for testing thin film materials and application to Al and Al (Si)". PhD thesis, Université catholique de Louvain, 2012.

[39] Gayatri K Cuddalorepatta et al. "Measurement of the stress-strain behavior of freestanding ultra-thin films". In: *Materialia* 9 (2020), p. 100502.

[40] Shaoning Lu, Jaehyun Chung, and Rodney S Ruoff. "Controlled deposition of nanotubes on opposing electrodes". In: *Nanotechnology* 16.9 (2005), p. 1765.

[41] ZL Xiao et al. “Fabrication of alumina nanotubes and nanowires by etching porous alumina membranes”. In: *Nano Letters* 2.11 (2002), pp. 1293–1297.

[42] Ehsan Hosseinian and Olivier N Pierron. “Quantitative in situ TEM tensile fatigue testing on nanocrystalline metallic ultrathin films”. In: *Nanoscale* 5.24 (2013), pp. 12532–12541.

[43] Yong Zhu et al. “Mechanical properties of vapor- liquid- solid synthesized silicon nanowires”. In: *Nano letters* 9.11 (2009), pp. 3934–3939.

[44] Yong Zhang et al. “Piezoresistivity Characterization of Synthetic Silicon Nanowires Using a MEMS Device”. In: *Journal of Microelectromechanical Systems* 20.4 (2011), pp. 959–967. DOI: 10.1109/JMEMS.2011.2153825.

[45] Bei Peng et al. “Measurements of near-ultimate strength for multiwalled carbon nanotubes and irradiation-induced crosslinking improvements”. In: *Nature nanotechnology* 3.10 (2008), pp. 626–631.

[46] Ravi Agrawal, Bei Peng, and Horacio D Espinosa. “Experimental-computational investigation of ZnO nanowires strength and fracture”. In: *Nano letters* 9.12 (2009), pp. 4177–4183.

[47] Lisa Y Chen et al. “Lattice anharmonicity in defect-free Pd nanowhiskers”. In: *Physical review letters* 109.12 (2012), p. 125503.

[48] Yogeeswaran Ganesan et al. “Effect of nitrogen doping on the mechanical properties of carbon nanotubes”. In: *Acs Nano* 4.12 (2010), pp. 7637–7643.

[49] JP Liebig et al. “A flexible method for the preparation of thin film samples for in situ TEM characterization combining shadow-FIB milling and electron-beam-assisted etching”. In: *Ultramicroscopy* 171 (2016), pp. 82–88.

[50] RC Hugo and RG Hoagland. “The kinetics of gallium penetration into aluminum grain boundaries—in situ TEM observations and atomistic models”. In: *Acta materialia* 48.8 (2000), pp. 1949–1957.

[51] Wikipedia contributors. *Dielectrophoresis — Wikipedia, The Free Encyclopedia*. https://en.wikipedia.org/w/index.php?title=Dielectrophoresis&oldid=1021981165. [Online; accessed 18-July-2021]. 2021.

[52] Md Amanul Haque and MTA Saif. “In situ tensile testing of nanoscale freestanding thin films inside a transmission electron microscope”. In: *Journal of Materials Research* 20.7 (2005), pp. 1769–1777.

[53] Md Amanul Haque and MT A Saif. “Mechanical behavior of 30–50 nm thick aluminum films under uniaxial tension”. In: *Scripta Materialia* 47.12 (2002), pp. 863–867.

[54] Jong H Han and M Taher A Saif. “In situ microtensile stage for electromechanical characterization of nanoscale freestanding films”. In: *Review of Scientific Instruments* 77.4 (2006), p. 045102.

[55] Frédéric Mompiou et al. “Inter-and intragranular plasticity mechanisms in ultrafine-grained Al thin films: An in situ TEM study”. In: *Acta materialia* 61.1 (2013), pp. 205–216.

[56] John Anthony Sharon et al. “Discerning size effect strengthening in ultrafine-grained Mg thin films”. In: *Scripta Materialia* 75 (2014), pp. 10–13.

[57] Sébastien Gravier et al. “New on-chip nanomechanical testing laboratory-applications to aluminum and polysilicon thin films”. In: *Journal of microelectromechanical systems* 18.3 (2009), pp. 555–569.

[58] M-S Colla et al. “High strength-ductility of thin nanocrystalline palladium films with nanoscale twins: on-chip testing and grain aggregate model”. In: *Acta Materialia* 60.4 (2012), pp. 1795–1806.

[59] B.R.N As Biology Revision Notes. *Electron microscopes*. `https://asbiologyrevision.files.wordpress.com/2015/02/fig04.gif`. [Online; accessed 20-July-2021]. 2015.

[60] Marc Legros. “In situ mechanical TEM: Seeing and measuring under stress with electrons”. In: *Comptes Rendus Physique* 15.2-3 (2014), pp. 224–240.

[61] P Castany and Marc Legros. “Preparation of H-bar cross-sectional specimen for in situ TEM straining experiments: A FIB-based method applied to a nitrided Ti–6Al–4V alloy”. In: *Materials Science and Engineering: A* 528.3 (2011), pp. 1367–1371.

[62] Khaled Bataineh. “Development of precision tem holder assemblies for use in extreme environments”. PhD thesis. University of Pittsburgh, 2005.

[63] J Pelissier and P Debrenne. “In situ experiments in the new transmission electron microscopes”. In: *Microscopy Microanalysis Microstructures* 4.2-3 (1993), pp. 111–117.

[64] Marc Legros, Martiane Cabié, and Daniel S Gianola. “In situ deformation of thin films on substrates”. In: *Microscopy research and technique* 72.3 (2009), pp. 270–283.

[65] Bruker. *TEM Picoindenter Series: Hysitron PI 95*. `https://www.bruker.com/en/products-and-solutions/test-and-measurement/nanomechanical-instruments-for-sem-tem/hysitron-pi-95-tem-picoindenter.html`. [Online; accessed 15-August-2021]. 2021.

[66] Warren J MoberlyChan et al. “Fundamentals of focused ion beam nanostructural processing: Below, at, and above the surface”. In: *MRS bulletin* 32.5 (2007), pp. 424–432.

[67] Joachim Mayer et al. “TEM sample preparation and FIB-induced damage”. In: *MRS bulletin* 32.5 (2007), pp. 400–407.

[68] Ivo Utke, Patrik Hoffmann, and John Melngailis. “Gas-assisted focused electron beam and ion beam processing and fabrication”. In: *Journal of Vacuum Science & Technology B: Microelectronics and Nanometer Structures Processing, Measurement, and Phenomena* 26.4 (2008), pp. 1197–1276.

[69] T Ishitani et al. “Implanted gallium-ion concentrations of focused-ion-beam prepared cross sections”. In: *Journal of Vacuum Science & Technology B: Microelectronics and Nanometer Structures Processing, Measurement, and Phenomena* 16.4 (1998), pp. 1907–1913.

[70] DS Gianola et al. “Stress-assisted discontinuous grain growth and its effect on the deformation behavior of nanocrystalline aluminum thin films”. In: *Acta Materialia* 54.8 (2006), pp. 2253–2263.

[71] Fredrick Madaraka Mwema et al. “Properties of physically deposited thin aluminium film coatings: A review”. In: *Journal of alloys and compounds* 747 (2018), pp. 306–323.

[72] Sami Franssila. *Introduction to microfabrication*. John Wiley & Sons, 2010.

[73] Winfab Wiki. *Physical Vapor Deposition: Evaporation*. `https://sites.uclouvain.be/winfab/NEW_website/dokuwiki/doku.php?id=techniques:pvd`. [Online; accessed 11-May-2021]. 2018.

[74] HF Winters and JW Coburn. “The etching of silicon with XeF2 vapor”. In: *Applied Physics Letters* 34.1 (1979), pp. 70–73.

[75] G Deokar et al. “Towards high quality CVD graphene growth and transfer”. In: *Carbon* 89 (2015), pp. 82–92.

[76] Xuesong Li et al. “Large-area synthesis of high-quality and uniform graphene films on copper foils”. In: *science* 324.5932 (2009), pp. 1312–1314.

[77] Vahid Samaee et al. “Dislocation driven nanosample plasticity: new insights from quantitative in-situ TEM tensile testing”. In: *Scientific reports* 8.1 (2018), pp. 1–11.

[78] Engineering 360. *An Inside Look at Carbon Fiber (and How It Can Change the Planet)*. `https://insights.globalspec.com/article/6620/an-inside-look-at-carbon-fiber-and-how-it-can-change-the-planet`. [Online; accessed 10-August-2021]. 2017.

[79] Tianfu Zhang et al. “Influence of reaction with XeF_2 on surface adhesion of Al and Al_2O_3 surfaces”. In: *Applied Physics Letters* 93.14 (2008), p. 141905.

Appendix A

A.1 Process step for the "mounting" of specimen by co-fabrication.

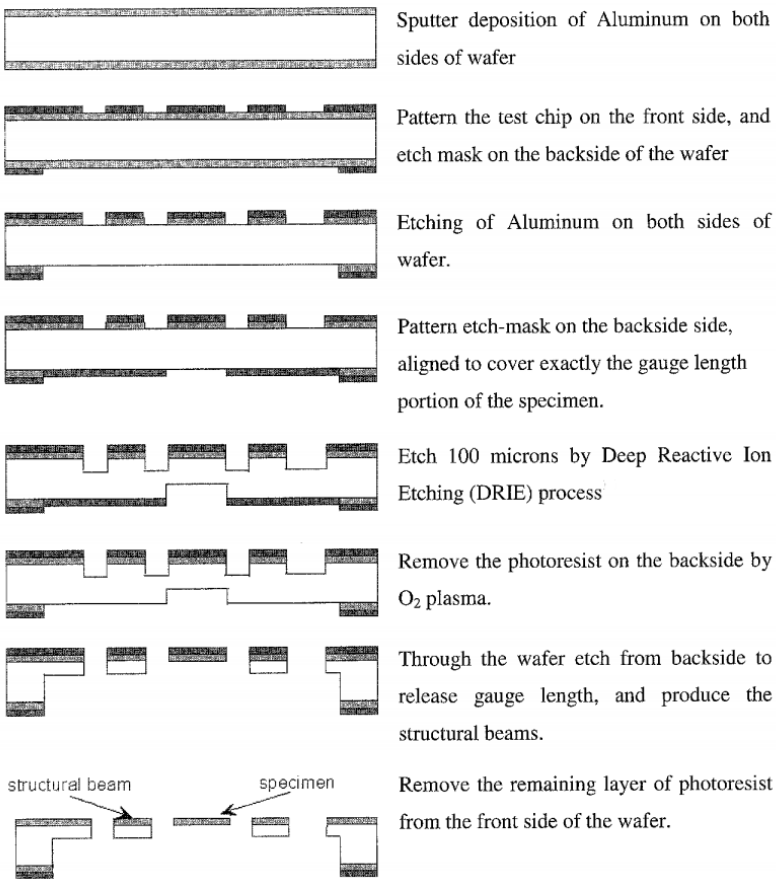

Figure A.1: Schematic diagram of the process flow for the fabrication of the MEMS testing device with a co-fabricated specimen by **Haque and Saif**. [26]

A.2 Sputtering parameter for alumina and aluminum thin film deposition

Material	Al_2O_3	Al
Target	Al	Al
0_2 [sccm]	3	0
N_2 [sccm]	0	0
Ar [sccm]	22	25
Pressure	1.2 mTorr	1.2 mTorr
Current	1.45 W	1.45 W
Voltage	478 V	478 V
Clean time	5' + 3'	5'
Deposition time	3',06"	4',33"
Temperature	RT	RT
Thickness	35nm	35nm
DC/RF	DC	DC
Base pressure	2.10^{-6} Torr	2.10^{-6} Torr

Table A.1: Sputtering parameter for alumina and aluminum deposition

Appendix B

B.1 Profilometery result

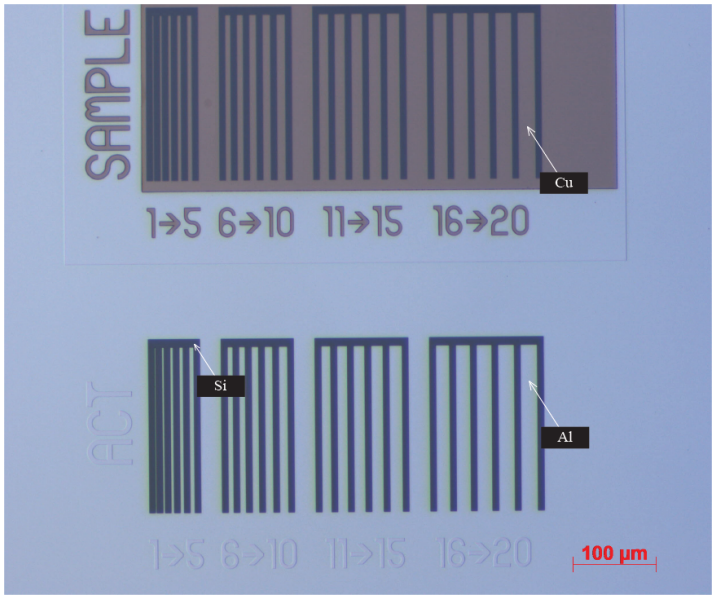

Figure B.1: Structures on the mask used to measure the thickness of the copper and aluminum thin film.

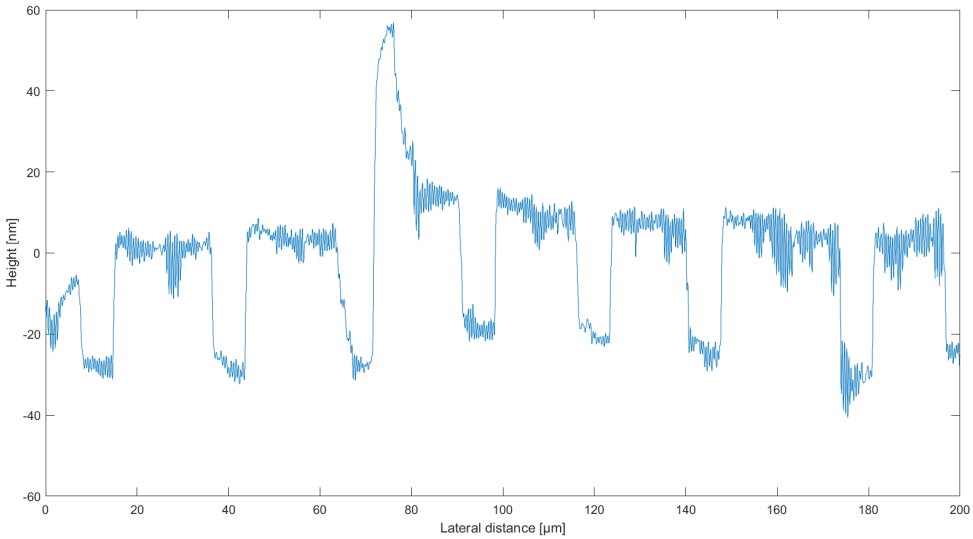

Figure B.2: Profilometry result for the measurement of the thickness of the copper sample.

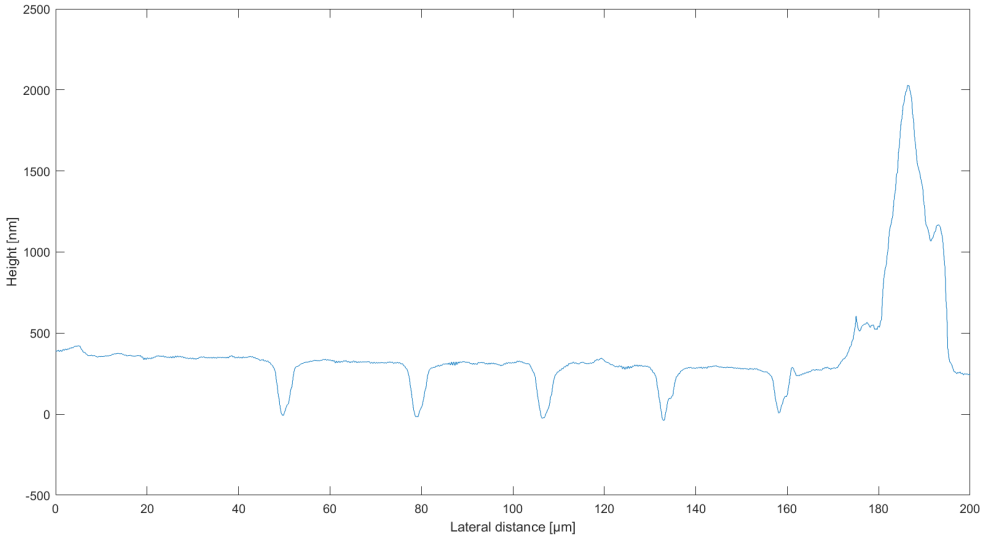

Figure B.3: Profilometry result for the measurement of the thickness of the aluminum frame.

B.2 Frame-Sample conceptual designs

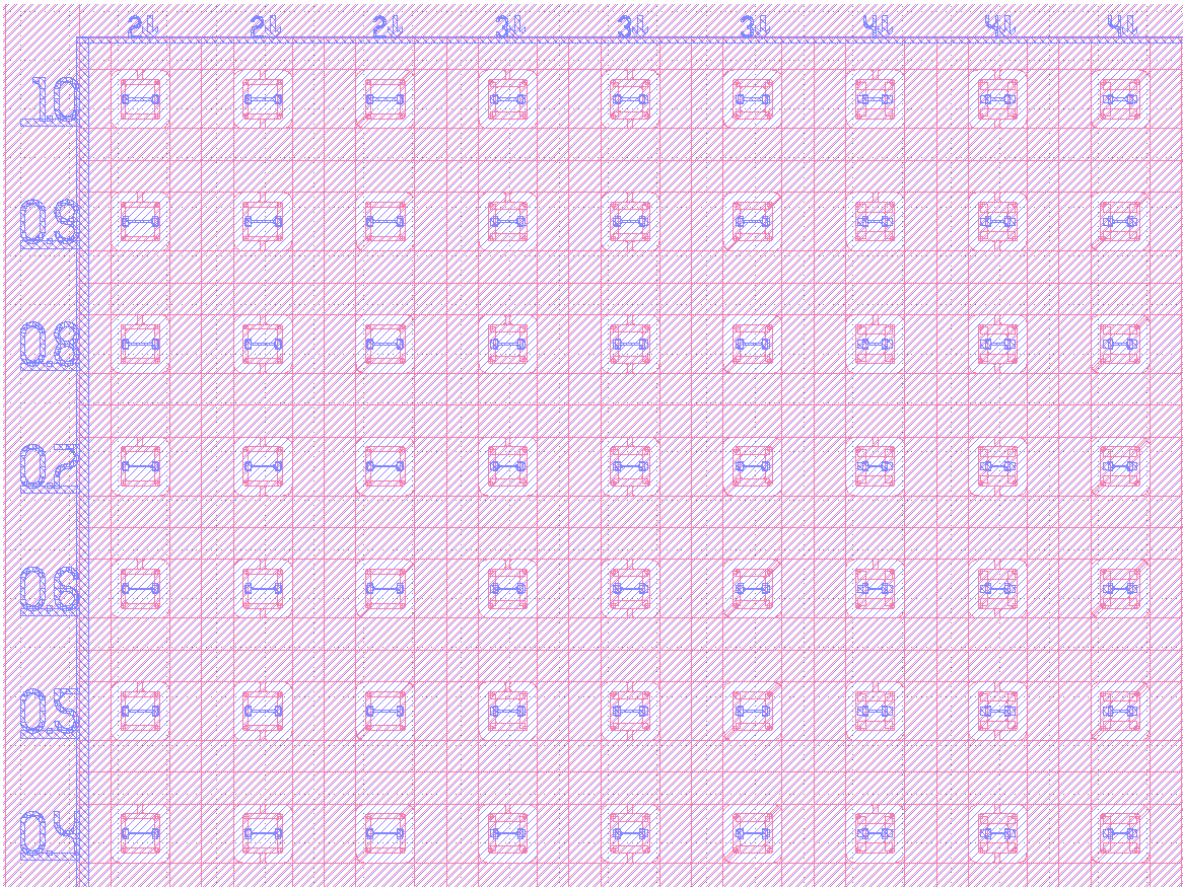

Figure B.4: Different conceptual designs for the frame-sample structure.

UNIVERSITÉ CATHOLIQUE DE LOUVAIN
École polytechnique de Louvain
Rue Archimède, 1 bte L6.11.01, 1348 Louvain-la-Neuve, Belgique | **www.uclouvain.be/epl**